Triphosphate Reorientation of the Incoming Nucleotide as a Fidelity Checkpoint in Viral RNA-dependent RNA Polymerases*

Received for publication, July 27, 2016, and in revised form, January 16, 2017 Published, JBC Papers in Press, January 18, 2017, DOI 10.1074/jbc.M116.750638

Xiaorong Yang[‡1], Xinran Liu[‡1], Derek M. Musser[‡], Ibrahim M. Moustafa[§], Jamie J. Arnold[§], Craig E. Cameron[§], and David D. Boehr[‡2]

From the Departments of [‡]Chemistry and [§]Biochemistry and Molecular Biology, Pennsylvania State University, University Park, Pennsylvania 16802

Edited by Charles E. Samuel

The nucleotide incorporation fidelity of the viral RNA-dependent RNA polymerase (RdRp) is important for maintaining functional genetic information but, at the same time, is also important for generating sufficient genetic diversity to escape the bottlenecks of the host's antiviral response. We have previously shown that the structural dynamics of the motif D loop are closely related to nucleotide discrimination. Previous studies have also suggested that there is a reorientation of the triphosphate of the incoming nucleotide, which is essential before nucleophilic attack from the primer RNA 3′-hydroxyl. Here, we have used ^{31}P NMR with poliovirus RdRp to show that the binding environment of the triphosphate is different when correct *versus* incorrect nucleotide binds. We also show that amino acid substitutions at residues known to interact with the triphosphate can alter the binding orientation/environment of the nucleotide, sometimes lead to protein conformational changes, and lead to substantial changes in RdRp fidelity. The analyses of other fidelity variants also show that changes in the triphosphate binding environment are not always accompanied by changes in the structural dynamics of the motif D loop or other regions known to be important for RdRp fidelity, including motif B. Altogether, our studies suggest that the conformational changes in motifs B and D, and the nucleoside triphosphate reorientation represent separable, "tunable" fidelity checkpoints.

Genome maintenance and propagation are dependent on faithful and efficient nucleic acid replication catalyzed by a large superfamily of template-directed polymerases (1). In each cycle of nucleotide addition, these polymerases must efficiently select the correct nucleotide that will properly base-pair with the template strand against a large pool of non-cognate nucleotides. The fidelity of nucleotide selection is essential for the integrity and proper expression of the genome. However, evolutionary processes require some level of incorrect nucleotide incorporation to generate the genetic diversity that allows a population of organisms to survive challenges from their environment. RNA viruses especially exemplify these ideas. For these viruses, it is now well established that the accuracy of RNA replication is a key determinant of viral virulence (2–6). Many RNA-dependent RNA polymerases (RdRps)[3] that are responsible for RNA viral genome replication operate near a limit of fine tuned mutation frequency, which optimally balances genetic diversity with overall genome integrity (7). Antiviral compounds like ribavirin that push the RdRp past an "error threshold" lead to the generation of too many replication errors and the loss of functional genetic information (7). However, variant RdRps with more stringent nucleotide selection criteria may not generate the genetic diversity that allows a virus population to escape the bottlenecks of the host's antiviral response. Indeed, it has been shown that viruses encoding variant RdRps with either higher or lower fidelity are attenuated in the host (2–6). In the case of poliovirus (PV), mice inoculated with these virus strains are also immunoprotected against lethal challenges of wild-type (WT) virus (3–5). An understanding of the fidelity mechanisms of RdRps would thus provide the framework for broad-spectrum antiviral strategies, including the design of new antiviral compounds and/or the generation of live, attenuated vaccine strains.

RdRps have the canonical "cupped right hand" structure with fingers, thumb, and palm subdomains and include seven highly conserved structural motifs, A–G, that are generally involved in interacting with RNA, nucleotide, and required metal ions (1) (Fig. 1). Recent X-ray crystal structures of PV (8, 9) and enterovirus 71 (10) RdRps have been especially informative concerning the conformational changes that take place during the nucleotide selection and incorporation processes. All parts of the incoming nucleoside triphosphate (NTP) are proposed to be involved in binding and selection. These crystal structures suggest that after initial base pairing between the incoming

* This work was supported by National Institutes of Health Grants AI104878 (to D. D. B.) and AI45818 (to C. E. C.). The authors declare that they have no conflicts of interest with the contents of this article. The content is solely the responsibility of the authors and does not necessarily represent the official views of the National Institutes of Health.

[1] Both authors contributed equally to this work.

[2] To whom correspondence should be addressed: Dept. of Chemistry, Pennsylvania State University, 107 Chemistry Bldg., University Park, PA 16802. Tel.: 814-863-8605; Fax: 814-863-0618; E-mail: ddb12@psu.edu.

[3] The abbreviations used are: RdRp, RNA-dependent RNA polymerase; PV, poliovirus; sym/sub-UA, symmetrical substrate RNA; MD, molecular dynamics; k_{pol}, maximum polymerase rate constant; $k_{pol}/K_{d(app)}$, catalytic efficiency; SDKIE, solvent deuterium kinetic isotope effect; HSQC, heteronuclear single quantum coherence; AMP-CPP, adenosine 5′-(α,β-methylene)triphosphate; α-P and γ-P, α- and γ-phosphate, respectively; 6-FAM, 6-carboxyfluorescein; PDB, Protein Data Bank.

NTP and the RNA template, the ribose hydroxyls interact with conserved residues Asp-238, Ser-288, and Asn-297 and other residues in motifs A and B (8–10) and induce a conformational change in this region. There is then a re-alignment of the NTP triphosphate and conserved residue Asp-233 around the two metal ions (10). Residues in motif F, including Lys-167 and Arg-174, are also involved in binding the triphosphate. We have proposed that structural changes in the motif D active-site loop bring in Lys-359 to act as the general acid to protonate the β-phosphate and generate a better pyrophosphate leaving group (11–13); this may be one of the final steps during nucleotide addition.

Previous mutagenesis experiments have confirmed the importance of conserved residues in motifs A, B, and D to RdRp function and fidelity (10, 12–19); similar studies for motif F residues have been largely lacking. Residues Lys-167 and Arg-174 probably play important functional roles, including initial nucleotide binding, realignment of the triphosphate for nucleophilic attack, and stabilization of the negative charges in the pentacoordinate transition state (9, 16). Previous studies have indicated that the R174K substitution in coxsackievirus B3 RdRp does not lead to viable virus (6), and amino acid substitutions elsewhere in motif F can alter fidelity in bovine diarrheal virus RdRp (20).

In this paper, we have used NMR and kinetic studies to provide insight into the roles of motif F residues in the fidelity mechanism of PV RdRp. ^{31}P NMR studies have allowed us to probe the NTP triphosphate conformation for both cognate and noncognate NTP, and [*methyl*-^{13}C]methionine NMR studies continue to provide insight into protein structural changes that accompany nucleotide selection, especially those associated with motifs B and D. The results with the motif F and previously identified fidelity variants suggest that triphosphate alignment is an important fidelity checkpoint but may be independent of conformational changes that occur in motifs B and D.

Results

^{31}P NMR Spectra Used to Monitor NTP Conformations in PV RdRp—We propose that there are (at least) four events to NTP selection and incorporation in RdRps: initial Watson-Crick base pairing with the RNA template, interactions between the NTP ribose hydroxyls and residues in motifs A and B to induce further conformational changes, a realignment of the NTP triphosphate involving residues in motifs A and F, and conformational changes in motif D to bring in the general acid Lys-359. Our previous NMR studies of PV RdRp using [*methyl*-^{13}C]Met-labeled protein established diagnostic probes for conformational changes in motifs B and D (also see Fig. 1*C*) (13, 21, 22). Here, we were interested in establishing probes for monitoring the NTP triphosphate conformation and alignment. Such probes would be important in evaluating the importance of motif F residues in RdRp catalysis and fidelity.

To examine more closely the triphosphate conformation and especially to compare conformations observed when correct *versus* incorrect nucleotide binds, we used ^{31}P NMR to probe the microenvironment surrounding the nucleotide and RNA binding pockets. Here, we have focused on the NTP triphosphate region of the ^{31}P NMR spectra, which gives insight into the triphosphate binding environment in the various RdRp complexes; only very minor differences were observed for the RNA peaks (0–1.2 ppm) in the various WT and variant RdRp complexes. Our studies took advantage of a symmetrical 10-mer RNA known as sym/sub-UA, which forms a 6-nucleotide duplex and 4-nucleotide overhangs (23) (Fig. 2*A*); the "UA" designates the first and second templating nucleobases. Using ^{31}P NMR, we were able to follow RdRp complex formation using our previously established procedures (13, 21) (Fig. 2*B*). In this procedure, we directly added 3′-dATP to our NMR sample, such that PV RdRp catalyzed phosphodiester bond formation to the RNA substrate but then prevented further nucleotide addition reactions due to the lack of the 3′-OH. Following the reaction, we passed the RdRp·RNA sample across a desalting spin column to eliminate excess 3′-dATP that might interfere with the binding of subsequent nucleotides. Following the desalting column, the majority of the signal related to the binding of 3′-dATP disappeared (Fig. 2*B*), indicating that the RdRp·RNA complex was now free to bind the next nucleotide. We then added a second nucleotide (*i.e.* UTP) that binds, but does not react, at the next register of the RNA (Fig. 2*A*). Passage across a second desalting column did not lead to the dissociation of the nucleotide (Fig. 2*B*). X-ray crystal structures had previously identified structural rearrangements that occur to "close" the active site upon nucleotide binding and addition (9). Presumably, these structural rearrangements and new interactions with the incoming NTP were responsible for retaining the UTP.

Consistent with this proposed procedure, additional peaks associated with the α-, β-, and γ-phosphates appeared upon adding the second nucleotide, UTP (Fig. 2*B*). The assignments of these peaks were consistent with those from similar protein-NTP binding studies (24–28). Close inspection of the ^{31}P spectrum indicated the presence of three intense peaks (δ −4.98, −10.08, and −18.65 ppm), which we assigned to the free NTP not bound to the protein because these chemical shifts were identical to NTP (in Mg^{2+}) by itself (*i.e.* no protein, RNA; Fig. 2*C*), and two minor peaks around the α- and γ-phosphate positions (δ −9.53 and −5.38 ppm), which we assigned to the NTP bound to the RdRp·RNA complex. After passage of the ternary RdRp·RNA·UTP complex across the desalting column, only the lower intensity, "protein-bound" peaks were retained (Fig. 2, *B* and *C*). The absence of a corresponding β-phosphate peak may reflect the low intensity of this peak and/or conformational exchange processes that would broaden out the β-phosphate peak associated with the protein-bound NTP.

Incorrect and Correct Incoming NTP Have Different Microenvironments—Some insight into the nature of the triphosphate binding pocket can be gained from comparisons of the ^{31}P NMR spectra of the RdRp·RNA·UTP complex and UTP by itself in the presence or absence of Mg^{2+} (Fig. 2*C*). As observed previously (28), binding of Mg^{2+} to free NTP led to similar downfield chemical shifts for both γ-P and α-P resonances (Fig. 2*C*). In the RdRp·RNA·UTP complex, the α-P peak of the protein-bound nucleotide (δ −9.53 ppm) was shifted even further downfield (Fig. 2*C*), potentially reflecting an even more electropositive environment in the active site with contributions from

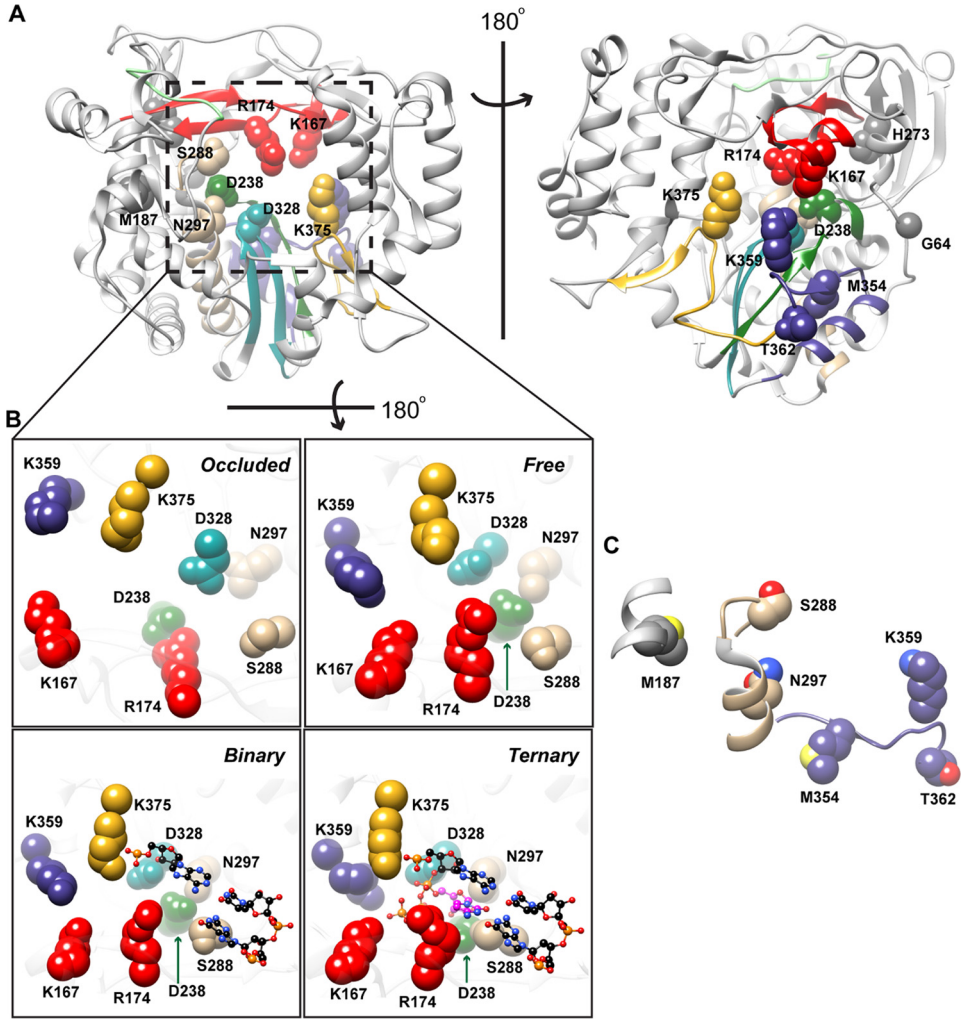

FIGURE 1. **Structural dynamics and interactions in the poliovirus RNA-dependent RNA polymerase.** *A*, overall structure of the poliovirus RdRp (PDB entry 3OL6) is shown with the conserved structural motifs *colored* (*dark green*, motif A; *tan*, motif B; *dark cyan*, motif C; *blue*, motif D; *golden yellow*, motif E; *red*, motif F; *light green*, motif G). Also highlighted are motif F residues Lys-167 and Arg-174 (*red*), motif D residues Lys-359 and Thr-362 (*blue*), and locations of other fidelity-altering substitutions (*i.e.* Gly-64 and His-273). *B*, conformational states of poliovirus RdRp based on X-ray crystal structures and MD simulations. The *boxed region* in *A* (*left*) is flipped 180° to improve clarity. The free state is in the absence of RNA and NTP (PDB entry 1RA6), the "binary" state is in the presence of RNA (PDB entry 3OL6), and postincorporation complex represents the "ternary" state (PDB entry 3OL7). All of the residues shown, including residues in motifs B (*i.e.* Ser-288 and Asn-297), D (*i.e.* Lys-359), and F (*i.e.* Lys-167 and Arg-174), undergo structural rearrangements from the binary to ternary complex. These residues make important interactions with the incoming NTP; Ser-288 and Asn-297 are important for ribose sugar recognition, and Lys-167, Arg-174, and Lys-359 are all predicted to interact with the triphosphate. We have also previously proposed that Lys-359 acts as a general acid to protonate the pyrophosphate leaving group. The "occluded" state is based on our previous MD simulations, which suggested that conserved residues that interact with the incoming NTP make interactions with each other, in the absence of NTP. *C*, NMR probes monitor rearrangements in the conserved structural motifs. The chemical shift positions of the ϵ-$^{13}CH_3$ Met-187 and Met-354 resonances are sensitive to structural rearrangements in motifs B and D (and other parts of the active site), where structural changes in these motifs are likely to be important for nucleotide selection. Residues are orientated similar to *A* (*left*).

both Mg^{2+} ions and basic amino acid side chains like Lys and Arg. Such interactions would also tend to create a more electrophilic α-P. In contrast, the γ-P peak of the protein-bound nucleotide was upfield shifted compared with the γ-P of Mg^{2+}-UTP and had a chemical shift similar to that of the γ-P of free UTP in the absence of Mg^{2+} (Fig. 2*C*). Although this finding might suggest that the γ-phosphate was no longer associated with Mg^{2+}, we do not believe such a scenario is likely. It is generally believed that the β- and γ-phosphates are associated with Mg^{2+} when binding the polymerase. Instead, a microenvironment may have been created around the γ-phosphate that was more electron-withdrawing compared with free Mg^{2+}-UTP, which may also lead to the weakening of the α-β phosphodiester bond; similar chemical shifts of the γ -P for free UTP and the RdRp·RNA·UTP complex were probably fortuitous.

To gain insights into how the binding of incorrect nucleotide differs from correct nucleotide, we also collected ^{31}P NMR spectra of the RdRp·RNA·2′-dUTP and RdRp·RNA·CTP complexes (Figs. 3 and 4). We first performed the RdRp·RNA·CTP experiments using different concentrations of CTP and at different temperatures. Here, we will focus first on the γ-P peak(s). As CTP is added, a second γ-P peak appears ($\delta \sim -5.8$ ppm at 4 mM), and then both γ-P peaks begin to shift upfield as more CTP is added ($\delta \sim -5.4$ and 6.2 ppm at 12 mM CTP and 293 K) (Fig. 3). As CTP is added, we also observe a broadening of the γ-P peaks (Fig. 3). To better understand what is happening, it is important to keep in mind that the incorrect nucleotide CTP is

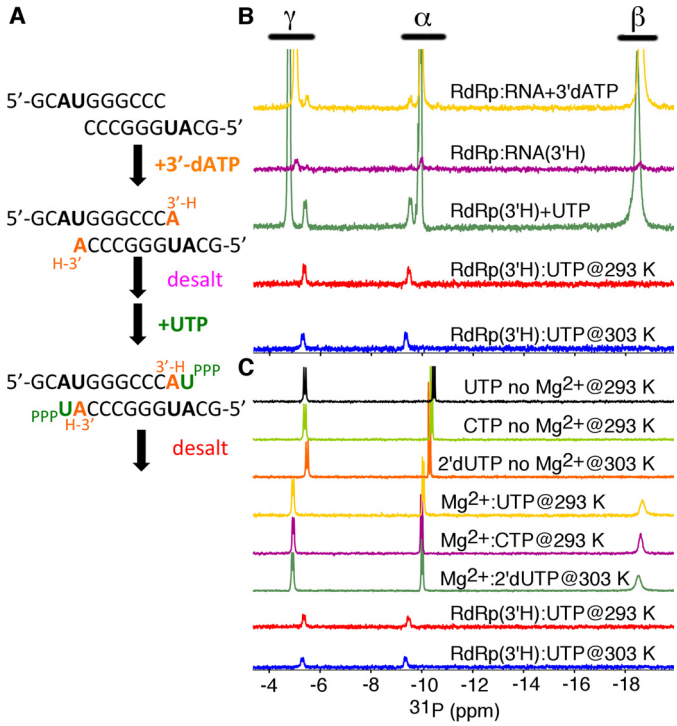

FIGURE 2. **Formation of RdRp RNA and nucleotide complexes can be followed using ^{31}P NMR.** *A*, the indicated 10-mer RNA can be used as a symmetrical substrate-template ligand. Incorporation of 3′-dATP terminates RNA synthesis, allowing the addition of a second nucleotide, UTP, to form the ternary RdRp·RNA(3′H)·UTP complex. Spin desalting columns can be used to remove excess free nucleotide. *B*, the triphosphates of the nucleotides can be detected using ^{31}P NMR. Not shown are the peaks for the phosphate backbone of the RNA. The spectra for the RdRp complexes at 293 K (RdRp·RNA+3′-dATP, RdRp·RNA(3′H), RdRp·RNA(3′H)+UTP, and RdRp·RNA(3′H)·UTP (desalted) shown in *golden yellow*, *magenta*, *green*, and *red*, respectively) and 303 K (RdRp·RNA(3′H)·UTP (desalted); *blue*) are shown. *C*, these spectra are also compared with the spectra for free NTPs in the absence and presence of Mg^{2+}, where temperatures are indicated on the plots. The assignments of the α-, β-, and γ-phosphates are also shown. Spectra for protein complexes were collected with 250 μM RdRp, 500 μM RNA, 3.1 mM 3′-dATP, and 4 mM UTP, where indicated, using buffer consisting of 10 mM HEPES, pH 8.0, 200 mM NaCl, 0.02% NaN_3, 5 mM MgCl, and 10 μM ZnCl. Spectra for free NTPs (*i.e.* in the absence of protein and RNA) were collected under the same buffer conditions using 2 mM NTP.

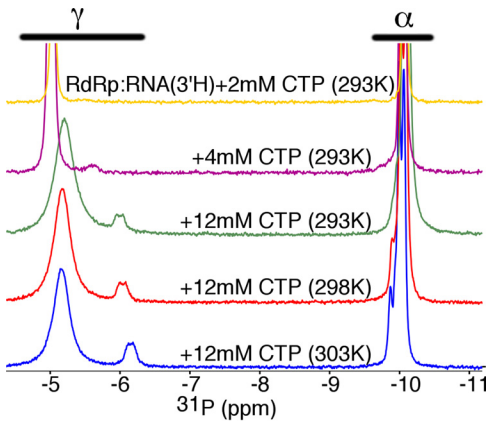

FIGURE 3. **Formation of ternary RdRp complexes with sym/sub-UA and the incorrect nucleotide CTP.** The spectra represent different concentrations of CTP added and/or different temperature, including +2 mM CTP/293 K (*golden yellow*), +4 mM CTP/293 K (*magenta*), +12 mM CTP/293 K (*green*), +12 mM CTP/298 K (*red*), and +12 mM CTP/303 K (*blue*). It should be noted that the incorrect nucleotide CTP has a lower affinity than correct nucleotide UTP, such that CTP is exchanging on/off the enzyme. This behavior is illustrated by the apparent chemical shift changes for the γ-P peak in response to different amounts of CTP and different temperatures. The spectra were collected with 250 μM RdRp, 500 μM RNA, 3.1 mM 3′-dATP, and the indicated CTP concentration using buffer consisting of 10 mM HEPES, pH 8.0, 200 mM NaCl, 0.02% NaN_3, 5 mM MgCl, and 10 μM ZnCl.

less tightly associated with the RdRp than correct UTP, and as such, the spectra reflect an exchange between "free" (in solution) and protein-bound CTP. When the time scale of this exchange is similar to that of the chemical shift differences between free and protein-bound CTP, then we observe chemical shift changes for both the apparent free and protein-bound γ-P peaks. In other words, the chemical shift of the free γ-P peak is "contaminated" with contributions from the chemical shift of the protein-bound γ-P peak (and vice versa), so the apparent free γ-P peak shifts toward the apparent protein-bound γ-P peak as more CTP is added. For variants with weaker association with CTP (*e.g.* K167R; see Fig. 4), the faster time scale of exchange can lead to the coalescence of the free and protein-bound peaks, leaving a single peak that represents a weighted population average of the underlying free and protein-bound peaks (see Ref. 29). A similar broadening/shifting of the α-P peaks does not occur because of the smaller chemical shift difference between the free and protein-bound α-P peaks. This behavior is also not observed for the WT RdRp·RNA·UTP complex probably because UTP is held more tightly and exchange on/off the enzyme is much slower. It should also be kept in mind that the ^{31}P NMR experiments were set up to minimize the signal from free (d)NTP, including a short recycle delay, precluding estimates of the proportion of incorrect (d)NTP bound to the protein and free in solution. For the γ-P peaks for the RdRp·RNA·CTP complex, we assign the more intense (at $\delta \sim -5.4$ ppm) and less intense (at $\delta \sim -6.2$ ppm) peaks to the free and protein-bound CTP, respectively.

There were substantial chemical shift differences in the ^{31}P NMR spectra of RdRp·RNA·UTP (Fig. 4*A*) and the RdRp·RNA·2′-dUTP (Fig. 4*B*) and RdRp·RNA·CTP (Fig. 4*C*) complexes, strongly suggesting that the orientation and/or binding microenvironments of the correct and incorrect nucleotides were substantially different between the two complexes. In particular, both the α-P (δ −9.84 ppm for RdRp·RNA·2′-dUTP and −9.87 ppm for RdRp·RNA·CTP) and the γ-P (δ −6.21 ppm for RdRp·RNA·2′-dUTP and −6.16 ppm for RdRp·RNA·CTP) peaks of the incorrect nucleotide were not as downfield shifted as that of the correct nucleotide (Fig. 4). Besides exchange on/off the enzyme, conformational motions of the triphosphate of the incorrect nucleotide when bound to the RdRp may also have contributed to peak broadening; structural studies of DNA polymerases suggest that incorrect NTP can fluctuate among an ensemble of conformations within the polymerase active site to prevent alignment and reaction with the primer 3′-OH (30–35).

Motif D and F Substitutions Change the Binding Environment of the Nucleotide Triphosphate—To gain more insight into the microenvironment surrounding the triphosphate moiety of the incoming nucleotide and the roles of amino acid residues interacting directly with the triphosphate, we also generated complexes for the K167R, R174K, and K359R variants (Fig. 4). Arg-174, Lys-359, and Lys-167 are proposed to interact primarily with the α-, β-, and γ-phosphates, respectively (Fig. 1*B*). The

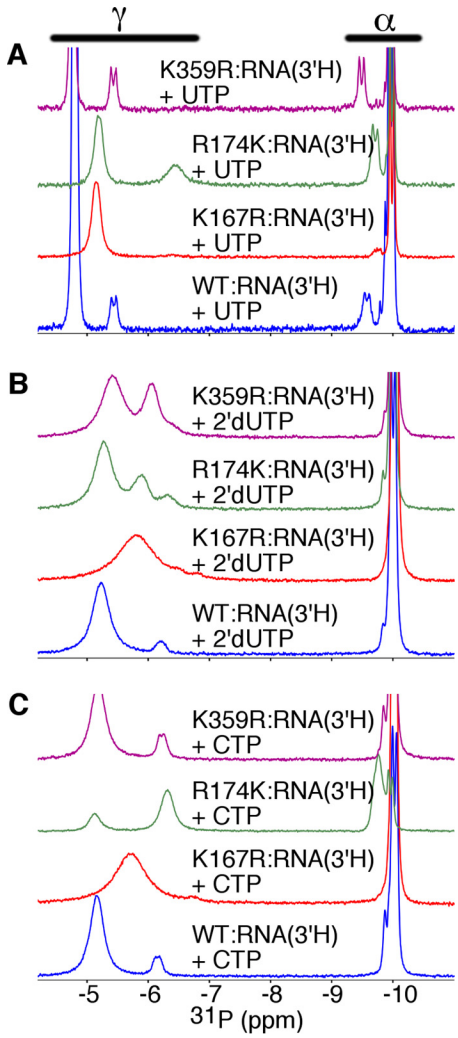

FIGURE 4. **Comparisons of RdRp·RNA bound with correct nucleotide (*i.e.* UTP) (*A*), bound with incorrect nucleotide with incorrect sugar (*i.e.* 2′-dUTP) (*B*), and bound with incorrect nucleotide with incorrect nucleobase (*i.e.* CTP) (*C*).** For the R174K variant, there were chemical shift changes for the α-P and γ-P peaks when both correct and incorrect incoming nucleotides were bound, suggesting that the microenvironment around the triphosphate was different from that of WT RdRp in both cases. For the K359R variant, there were chemical shift changes when correct nucleotide bound, consistent with the residue at position 359 making an interaction with the triphosphate in the "closed" conformation. Spectra were collected at 303 K with 250 μM RdRp, 500 μM RNA, and 4 mM UTP, 8 mM 2′-dUTP, or 12 mM CTP, using buffer consisting of 10 mM HEPES, pH 8.0, 200 mM NaCl, 0.02% NaN_3, 5 mM MgCl, and 10 μM ZnCl.

conservative amino acid changes should still allow these positively charged residues to interact with the NTP triphosphate, albeit in an altered fashion that could be monitored by ^{31}P NMR.

Arg-174 is probably important for the alignment of the α-phosphate for reaction with the primer 3′-OH. Consistent with the role of Arg-174 in interacting with the α-phosphate, the chemical shift for the protein-bound α-P was upfield shifted in the R174K variant (δ −9.74 ppm) compared with WT RdRp (δ −9.36 ppm). The chemical shift positions of the α-P and γ-P for the R174K·RNA·UTP and R174K·RNA·CTP complexes were remarkably similar (Fig. 4); only the relative intensities and widths of the peaks were different. The changes in peak intensities may just reflect the difference in the concentrations of the nucleotides used in these experiments (*i.e.* [UTP] = 4 mM; [CTP] = 12 mM) and different exchange rates on/off the enzyme. Intriguingly, the R174K·RNA·2′-dUTP complex (Fig. 4*B*) gave rise to three peaks associated with γ-P (δ −5.28, −5.89, and −6.32), suggesting that the γ-phosphate for the "bound" 2′-dUTP might fluctuate between two or more conformations.

We have proposed that binding of correct, but not incorrect, nucleotide results in a structural rearrangement in the motif D loop to bring Lys-359 into the active site to interact with the β-phosphate (13). If so, we expected that the K359R substitution would lead to changes in the ^{31}P NMR spectrum of the correct RdRp·RNA·UTP complex but not the RdRp complexes bound with incorrect nucleotide. Consistent with this proposal, the K359R substitution led to small upfield chemical shift changes in the α-P and γ-P peaks of the RdRp·RNA·UTP complex (δ −9.49 and −5.43 ppm; Fig. 4*A*) but did not lead to substantial chemical shift changes in the RdRp·RNA·CTP spectrum (δ −9.87 and −6.25 ppm; Fig. 4*C*) compared with the corresponding WT complexes. However, there was also a change in the γ-P peaks for the K359R·RNA·2′-dUTP spectrum (δ −5.40 and −6.03 ppm) compared with the WT complex (Fig. 4*B*). These changes may reflect different nucleotide exchange kinetics and/or changes to the binding microenvironment for 2′-dUTP once bound to the K359R variant.

The K167R substitution also led to differences in the spectra for the ternary complexes. In particular, there was one very broad γ-P peak for the RdRp·RNA·2′-dUTP and RdRp·RNA·CTP complexes, which probably reflects changes in the nucleotide exchange kinetics. In other words, exchange on/off the enzyme is fast compared with the chemical shift differences between free and protein-bound NTP, such that the single γ-P peak represents a weighted average of the free and protein-bound states. This proposal is consistent with the higher apparent nucleotide dissociation constants for the K167R variant compared with WT RdRp (see Table 1). The protein-bound peak intensities for the K167R·RNA·UTP complex were also quite weak, which might be indicative of decreased UTP binding and/or additional exchange processes on the enzyme that would broaden out these signals. These results were consistent with Lys-167 making important interactions with the triphosphate, which might be important for nucleotide binding affinity.

The R174K Substitution Also Prevents Motif D Structural Rearrangements as Monitored by Protein NMR—The ^{31}P NMR spectra for the K167R, R174K, and K359R variants indicated that these amino acid substitutions lead to changes in how the triphosphate interacts with the RdRp. We also collected NMR spectra of [*methyl*-^{13}C]Met-labeled RdRp to gain insight into how these amino acid substitutions change RdRp structural dynamics. In particular, we have previously noted that Met-354 is a good reporter of any structural and/or dynamic changes in the motif D loop (see also Fig. 1*C*), which we propose are important for repositioning Lys-359 for catalysis. Chemical shift changes to Met-354 are generally accompanied by chemical shift changes to other informative resonances, such as Met-6, Met-74, and Met-225 (Fig. 5).

TABLE 1
Comparison of the kinetic constants of nucleotide incorporation for variant and WT RdRp enzymes

Variant	Metal	NTP	k_{pol}	$K_{d(app)}$	$k_{pol}/K_{d(app)}$
			s^{-1}	μM	$\mu M^{-1}\ s^{-1}$
Correct NTP					
WT	Mg^{2+}	ATP	59 ± 1	36 ± 2	1.6
		ATP (D_2O)[a]	27 ± 1	15 ± 1	1.8
	Mn^{2+}	ATP	16 ± 1	1.7 ± 0.1	9.4
		ATP (D_2O)[a]	5.3 ± 0.1[b]	ND[c]	ND
K167M	Mg^{2+}	ATP	26 ± 0.2	683 ± 29	3.8×10^{-2}
K167R	Mg^{2+}	ATP	56 ± 1	27 ± 1	2.1
		ATP (D_2O)[a]	12 ± 1	7.5 ± 1.0	1.6
	Mn^{2+}	ATP	21 ± 1	4.1 ± 0.3	5.3
		ATP (D_2O)[a]	3.1 ± 0.1	ND	ND
R174K	Mg^{2+}	ATP	4.2 ± 0.2	19 ± 4	0.22
		ATP (D_2O)[a]	1.7 ± 0.1	2.5 ± 0.1	0.68
	Mn^{2+}	ATP	1.7 ± 0.1	0.20 ± 0.03	8.5
		ATP (D_2O)[a]	0.40 ± 0.01[b]	ND	ND
K359L	Mg^{2+}	ATP	0.62 ± 0.01	272 ± 15	2.3×10^{-3}
R174K/K359L	Mg^{2+}	ATP	0.011 ± 0.001	148 ± 24	7.4×10^{-5}
Incorrect sugar					
WT	Mg^{2+}	2′-dATP	0.89 ± 0.01	134 ± 4	6.6×10^{-3}
	Mn^{2+}	2′-dATP	7.4 ± 0.1	6.1 ± 0.1	1.2
K167R	Mg^{2+}	2′-dATP	3.4 ± 0.1	321 ± 25	1.1×10^{-2}
	Mn^{2+}	2′-dATP	15 ± 1	9.5 ± 1.0	1.6
R174K	Mg^{2+}	2′-dATP	$2.4 \pm 0.1 \times 10^{-4}$	26 ± 6	9.2×10^{-7}
	Mn^{2+}	2′-dATP	0.5	7.6 ± 0.5	6.6×10^{-2}
Incorrect nucleobase					
WT	Mg^{2+}	GTP	0.011 ± 0.001	142 ± 15	7.7×10^{-5}
	Mn^{2+}	GTP	0.80 ± 0.01	98 ± 3	8.2×10^{-3}
K167R	Mg^{2+}	GTP	$3.7 \pm 0.1 \times 10^{-2}$	223 ± 20	1.7×10^{-4}
	Mn^{2+}	GTP	1.9 ± 0.1	168 ± 19	1.1×10^{-2}
R174K	Mg^{2+}	GTP	$3.0 \pm 0.1 \times 10^{-5}$[d]	ND	ND
	Mn^{2+}	GTP	0.11 ± 0.01	57 ± 5	1.9×10^{-3}

[a] Kinetic constants were determined in D_2O solvent.
[b] k_{pol} was estimated using [ATP] = 20 μM (*i.e.* $>10 \times K_{d(app)}$ in H_2O and Mn^{2+}).
[c] ND, no data.
[d] k_{pol} was estimated using [GTP] = 500–2000 μM (*i.e.* $>5 \times K_{d(app)}$ for WT RdRp).

For the K167R variant, there were no substantial chemical shift differences compared with the corresponding WT complexes (Fig. 5, *A*–*C*), suggesting that the overall protein conformation was not substantially affected by this amino acid change. In contrast, binding of the correct UTP nucleotide to the R174K variant did not result in the same chemical shift changes as observed for WT RdRp (Fig. 5*D*). In fact, the chemical shift changes induced by binding of correct and incorrect nucleotides were similar for the R174K variant and similar to those changes induced by the binding of the incorrect nucleotide to WT RdRp (Fig. 5, *E* and *F*). These findings suggest that conformational changes in the motif D loop and other associated structural changes were severely impaired in the R174K variant. Altogether, these findings are consistent with our previous results that indicated that the α- and β-phosphates but not the γ-phosphate of the incoming nucleotide is required for the conformational changes in motif D and surrounding areas (13).

Motif F Substitutions Also Lead to Changes around Motif B—We have also previously used the Met-187 resonance as a probe to support molecular dynamics (MD) simulations suggesting that motif B and nearby regions fluctuate between conformations competent for and occluded from NTP binding (see also Fig. 1*C*) (22). In the occluded conformation (Fig. 1*B*), Arg-174 is involved in a salt-bridging interaction with Asp-238, such that this interaction and others must be broken before the RdRp·RNA complex can bind NTP (22); Met-187 is a reporter of these interactions and rearrangements (22). For the WT protein, there were distinct chemical shift changes when correct UTP and incorrect CTP were added to the RdRp·RNA complex (Fig. 6*A*). The K167R, R174K, and K359R substitutions all led to changes to the Met-187 resonances, especially for the RdRp·RNA and RdRp·RNA·CTP complexes, suggesting that these substitutions have long range effects on the structure/dynamics of motif B and surrounding regions (Fig. 6). In contrast, the Met-187 resonances were very similar for the RdRp·RNA·UTP complexes (Fig. 6). The one exception was for the R174K variant, in which there were two additional resonances, where one of these overlapped that for the R174K RNA·CTP complex (Fig. 6*C*). Altogether, these results suggested that motif B and surrounding regions can attain a similar conformation when correct NTP binds for all variants, but the conformations in the absence of NTP or in the presence of incorrect NTP may differ.

Other changes to the Met-187 resonances were also informative. There were two resonances for the K167R RdRp·RNA·CTP complex, with one of those resonances more similar to what was observed for the K167R RdRp·RNA·UTP complex (Fig. 6*B*). There was no apparent Met-187 resonance for the R174K RdRp·RNA complex, suggesting conformational exchange on the intermediate NMR time scale (Fig. 6*C*). One potential explanation would be that the R174K substitution disrupts the interactions with Asp-238, such that the conformational exchange kinetics between NTP binding-competent and occluded conformations was moved to the intermediate NMR time scale. Finally, the Met-187 resonances for the K359R ternary complexes had similar chemical shift positions, in contrast to what was observed for WT RdRp (Fig. 6*D*). A comparable

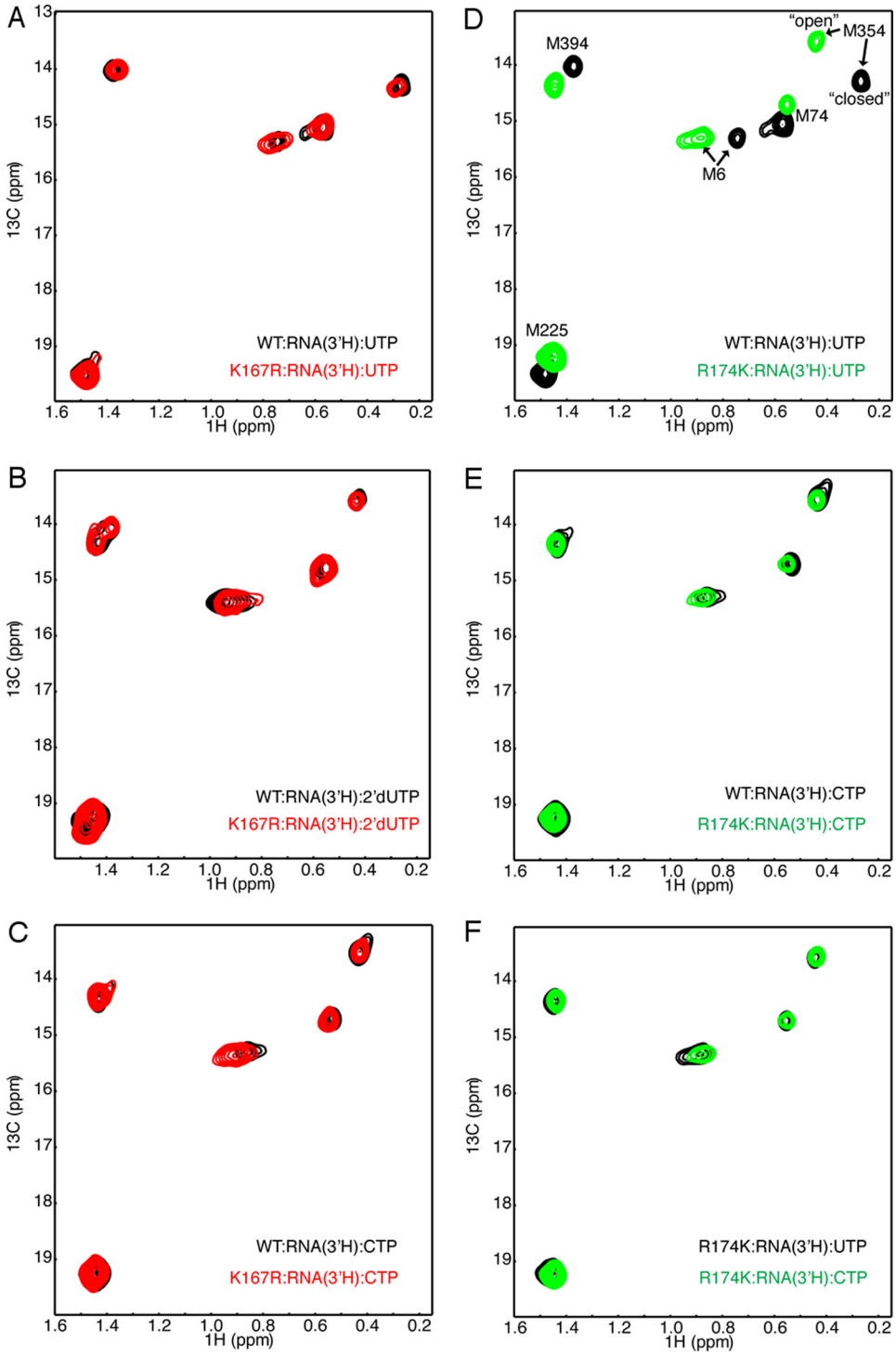

FIGURE 5. **Amino acid substitutions at triphosphate-interacting positions can change RdRp structural dynamics at motif D.** *A–E*, comparison of [*methyl*-^{13}C]Met HSQC spectra between WT (*black*), K167R (*red*), and R174K (*green*) RdRp bound with RNA lacking a 3′-OH and correct UTP nucleotide or incorrect 2′-dUTP or incorrect CTP nucleotide. The chemical shift signatures for R174K and WT RdRp bound with RNA and correct UTP nucleotide were quite different. More insight was gleaned from the finding that the spectra for the R174K variant bound with correct UTP (*black*) and incorrect CTP (*green*) nucleotides were nearly identical (*F*). This finding suggests that the R174K variant was impaired in its ability to form a "closed" conformation like WT RdRp. Spectra were collected at 293 K using 250 μM RdRp with 500 μM RNA and 4 mM UTP (12 mM UTP for the R174K variant), 8 mM 2′-dUTP, or 12 mM CTP and a D_2O-based buffer consisting of 10 mM HEPES, pH 8.0, 200 mM NaCl, 0.02% NaN_3, 5 mM MgCl, and 10 μM ZnCl.

scenario was observed previously for the low fidelity H273R variant, in which the H273R variant was proposed to favor the NTP binding-competent conformation and did not show any differences for the Met-187 resonance between the RdRp·RNA·UTP and RdRp·RNA·CTP complexes (22).

The R174K Substitution Reduces Catalytic Efficiency and Increases Nucleotide Selection Fidelity—Not surprisingly, the ^{31}P and [*methyl*-^{13}C]Met spectra suggested that conserved amino acid substitutions at residues proposed to interact with the NTP triphosphate alter the nucleotide binding kinetics

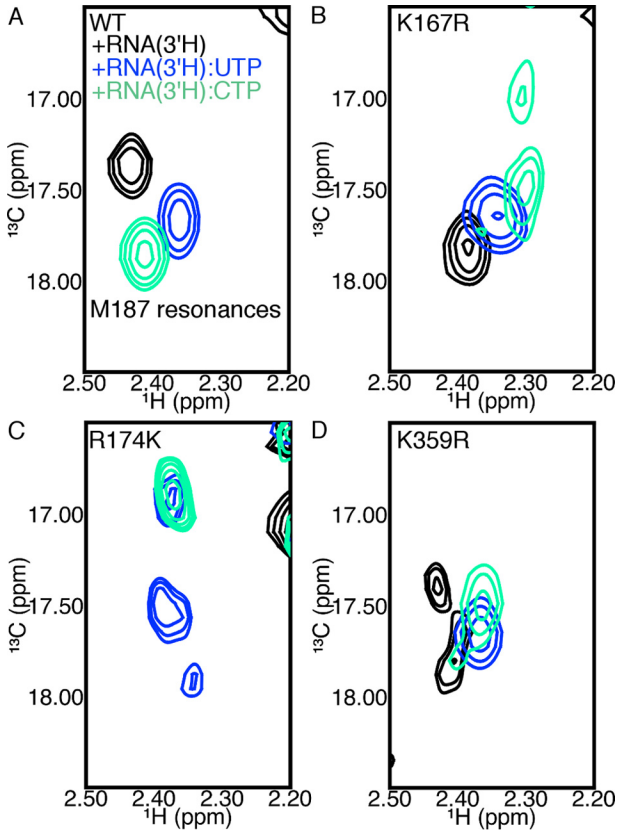

FIGURE 6. **Amino acid substitutions at triphosphate-interacting positions change RdRp structural dynamics around motif B.** It was shown previously that the Met-187 resonance is a reporter of conformational changes in motif B, including those changes associated with RNA and NTP binding (22). Met-187 resonances from [*methyl*-^{13}C]Met HSQC spectra are shown for RdRp bound to sym/sub-UA lacking a 3′-OH (*black*), bound to RNA lacking a 3′-OH and correct UTP (*blue*), and bound to RNA lacking a 3′-OH and incorrect CTP (*green*) for WT (*A*), K167R (*B*), R174K (*C*), and K359R (*D*) complexes. Spectra were collected at 293 K using 250 μM RdRp with 500 μM RNA and 4 mM UTP (12 mM UTP for the R174K variant), 8 mM 2′-dUTP, or 12 mM CTP and a D_2O-based buffer consisting of 10 mM HEPES, pH 8.0, 200 mM NaCl, 0.02% NaN_3, 5 mM MgCl, and 10 μM ZnCl.

and/or conformation. To gain more insight, we analyzed the ability of RdRp variants to bind RNA and assemble into catalytically competent complexes and measured the maximum polymerase rate constant (k_{pol}) and the apparent dissociation constant for the incoming nucleotide ($K_{d(app)}$). To compare RNA binding between variant and WT RdRp, we monitored interactions with 6-carboxyfluorescein (6-FAM)-labeled sym/sub-UA RNA using a fluorescence polarization assay (Table 2). This assay indicated that most substitutions at Lys-167, Arg-174, and Lys-359 had little effect on RNA binding affinity (Table 2). The sole exception was the R174L substitution, and the large decrease in RNA binding affinity precluded further assessment of this variant.

To ensure that the variants could assemble efficiently on the sym/sub-UA template and catalyze phosphodiester bond formation with the incoming nucleotide, we initiated the reaction with the addition of RdRp and followed RNA synthesis over various time points (Fig. 7*A*). The assay indicated that the variants could assemble for catalysis in a similar time frame as WT RdRp. We also compared the stabilities of the RdRp·RNA complexes between variant and WT RdRps by incubating RdRp enzyme with labeled sym/sub-UA for 90 s to allow the

TABLE 2
Interactions between variant and WT RdRps and sym/sub-UA RNA

RdRp	K_d	k_d
	nM	$\times 10^{-4}$ s^{-1}
WT	575 ± 68	4.0 ± 0.2
K167M	254 ± 28	1.4 ± 0.6
K167R	767 ± 203	3.5 ± 0.1
R174K	603 ± 35	11 ± 1
R174L	1951 ± 304	5.7 ± 0.8
K359L	397 ± 28	1.4 ± 0.1
R174K/K359L	1024 ± 95	4.2 ± 0.7

RdRp·RNA binary complexes to form before the addition of excess unlabeled sym/sub-UA to trap free and dissociating enzyme (Fig. 7*B*). ATP was then added at various times after the addition of the unlabeled sym/sub-UA, and the reaction was quenched 30 s later. This assay indicated that the R174K variant dissociated more quickly from the labeled RNA compared with WT RdRp (Table 2). Nonetheless, the RdRp·RNA complex for R174K RdRp was deemed sufficiently stable for our single nucleotide incorporation assays to measure k_{pol} and $K_{d(app)}$ values. It is important to note that we also checked the RdRp catalytic activity under buffer conditions that we used for the ^{31}P and [*methyl*-^{13}C]Met NMR experiments, which did not reveal any substantial differences compared with the buffer system we used for our kinetic assays (Fig. 8).

The K167R substitution had little effect on the k_{pol} and $K_{d(app)}$ values for correct nucleotide incorporation (*i.e.* ATP, in the presence of Mg^{2+}) but led to increases in k_{pol}, $K_{d(app)}$, and catalytic efficiency ($k_{pol}/K_{d(app)}$) for incorrect nucleotide incorporation compared with WT RdRp (Table 1). As mentioned above, the change in $K_{d(app)}$ for incorrect nucleotide may help to explain the broader peaks in the ^{31}P NMR spectrum for the K167R·RNA·2′-dUTP and K167R·RNA·CTP complexes (Fig. 4), which suggests a change in the binding on/off rates. These results also indicate that the K167R variant is less able to discriminate against incorrect nucleotide and has lower fidelity compared with WT RdRp. The K167M variant also had a substantial increase in the $K_{d(app)}$ for correct nucleotide. The higher $K_{d(app)}$ values precluded further kinetic assessment of incorrect nucleotide incorporation for this variant.

Perhaps not surprisingly, the R174K variant led to a 14-fold drop in k_{pol} for correct nucleotide incorporation (*i.e.* ATP, in the presence of Mg^{2+}) compared with WT RdRp (Table 1). More remarkable was the finding that the change in k_{pol} was even more substantial for incorrect nucleotide incorporation, either with incorrect sugar (*i.e.* 2′-dATP) or incorrect nucleobase (*i.e.* GTP). Specifically, there were 3,700- and 370-fold drops in k_{pol} for 2′-dATP and GTP incorporation, respectively, compared with WT RdRp (k_{pol} for GTP was estimated based on using 1000 μM GTP (*i.e.* almost 10-fold greater than the $K_{d(app)}$ for WT RdRp; Table 1). These k_{pol} values also indicated that the R174K variant was more faithful (*i.e.* $k_{pol(correct)}/k_{pol(incorrect)}$ values were 17,500 and 140,000 for 2′-dATP and GTP, respectively) than WT RdRp ($k_{pol(correct)}/k_{pol(incorrect)}$ values were 70 and 5400 for 2′-dATP and GTP, respectively).

Metal and Solvent Effects Help to Gauge the Effects of Amino Acid Substitutions on the Prechemistry Conformational Change and Chemical Steps—To gain more insight into the effects of these amino acid substitutions, we also assayed the effects of

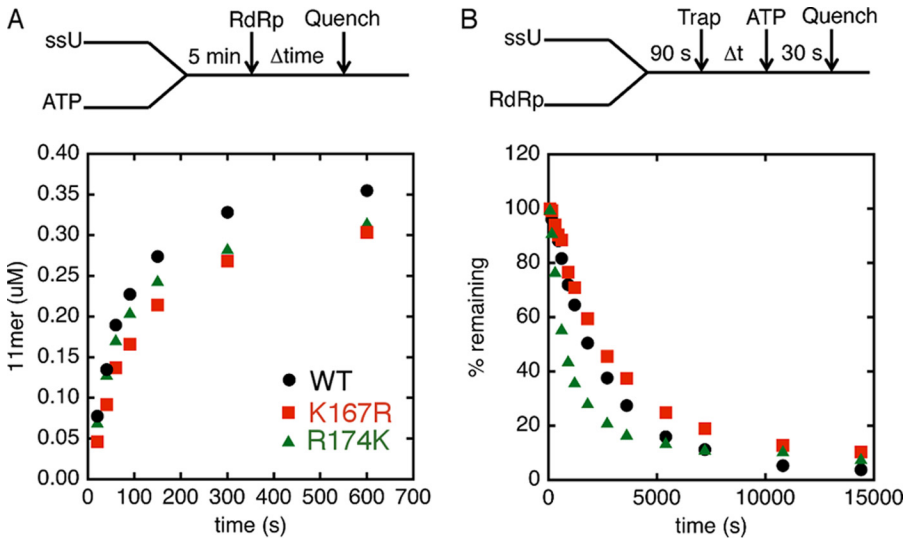

FIGURE 7. **Formation and stability of RdRp·RNA complexes is similar between WT RdRp and motif F variants.** *A*, RdRp·RNA·NTP assembly assay. Reactions were initiated by adding RdRp (1 μM) into sym/sub-UA (0.5 μM duplex) and ATP (500 μM), which were incubated at 30 °C for 5 min. At the indicated times, reactions were quenched by adding 25 mM EDTA. The results for the RdRp·RNA·NTP assembly assay are shown for WT (*black circles*), K167R (*red squares*), and R174K (*green triangles*). *B*, RdRp·RNA dissociation assay. RdRp and RNA were incubated at 30 °C for 90 s, at which time trap (100 μM unlabeled RNA) was added to the reaction buffer. After the indicated times, the reaction buffer was mixed with ATP (500 μM) and then quenched after 30 s by adding EDTA (25 mM). The results for the RdRp·RNA dissociation assay are shown for WT (*black circles*), K167R (*red squares*), and R174K (*green triangles*).

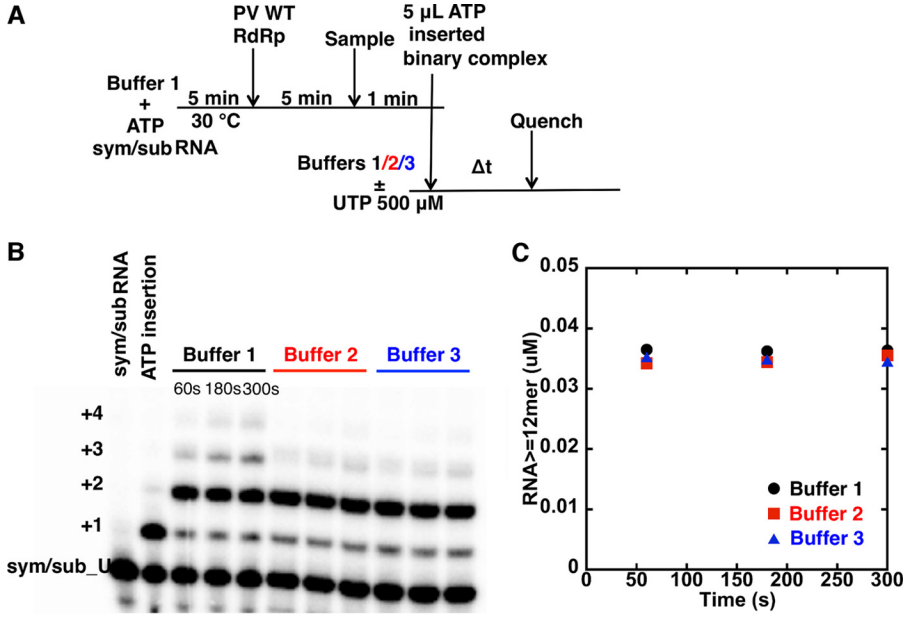

FIGURE 8. **UMP incorporation into sym/sub-UA is not affected by the composition of the buffers used for NMR experiments.** *A*, reaction scheme. Buffer 1 was preincubated with 500 μM ATP and 1 μM sym/sub-UA for 5 min, and then the reaction was initiated by the addition of 5 μM WT RdRp to incorporate AMP into sym/sub-UA. After 5 min, the AMP incorporated RdRp·RNA complexes were added into 500 μM UTP and buffers 1, 2, and 3, respectively, via a 1:10 ratio so that the final concentrations of RdRp, RNA, and ATP were 0.5, 0.1, and 50 μM, respectively. The reactions were then quenched at the indicated times by the addition of EDTA to a final concentration of 50 mM. *B*, products from reactions described in *A* were resolved by electrophoresis on a denaturing 23% polyacrylamide gel. *C*, comparison of UMP incorporation kinetics using buffers 1, 2, and 3. Buffer 1 contained 50 mM HEPES, pH 7.5, 10 mM β-mercaptoethanol, 5 mM $MgCl_2$, and 60 μM $ZnCl_2$; buffer 2 contained 10 mM HEPES, pH 8.0, 200 mM NaCl, 5 mM $MgCl_2$, 10 μM $ZnCl_2$, and 0.02% NaN_3 in 100% D_2O; and buffer 3 contained the same components as buffer 2 except that the final concentration of D_2O was 10%. All reactions were performed at 30 °C.

changing the metal ion and the solvent. In the presence of Mg^{2+}, the incorporation of correct nucleotide catalyzed by the WT enzyme is partially rate limited by both a prechemistry conformational change and the chemistry step itself (36). The prechemistry conformational change and the chemical step also both contribute to discrimination against nucleotide with incorrect sugar or incorrect nucleobase (36). In contrast, correct nucleotide incorporation catalyzed by the WT enzyme is more rate-limited by the chemical step in the presence of Mn^{2+}, presumably because the correct nucleotide more readily induces the prechemistry conformational change with this metal (37). However, the chemistry step is less discriminatory in the presence of Mn^{2+}, and the prechemistry step largely governs polymerase fidelity (37). The relative contribution of the chemistry step can also be assayed by performing the assays in D_2O, because the solvent deuterium kinetic isotope effect

(SDKIE; *i.e.* $k_{pol(H2O)}/k_{pol(D2O)}$) reports on proton transfer steps occurring during phosphodiester bond formation (11).

The SDKIEs for the K167R and R174K variants were higher than WT RdRp in the presence of Mg^{2+} (4.67 ± 0.40, 2.47 ± 0.05, and 2.19 ± 0.03 for K167R, R174K, and WT RdRp, respectively) or Mn^{2+} (6.77 ± 0.40, 4.25 ± 0.02, and 3.02 ± 0.03 for K167R, R174K, and WT RdRp, respectively) (Table 1). These results suggest that the K167R and R174K substitutions both decreased the rate of the chemistry step. Nucleotide discrimination for the K167R and R174K variants was more similar to that of WT RdRp in Mn^{2+} (*i.e.* $k_{pol(ATP)}/k_{pol(2'\text{-}dATP)}$ values are 1.4, 3.4, and 2.2 for K167R, R174K, and WT RdRp respectively; $k_{pol(ATP)}/k_{pol(GTP)}$ values are 11, 15, and 20) than Mg^{2+}. These results suggest that the differences in RdRp fidelity in the presence of Mg^{2+} are probably due to the K167R and R174K substitutions primarily affecting the chemical step for incorrect nucleotide incorporation, such that most of these effects disappear with Mn^{2+}.

Kinetic Experiments Indicate That the R174K Variant Exchanges Nucleotides More Readily—The NMR experiments suggested that the NTP and protein structural changes for R174K variant were substantially different from that observed for WT enzyme. To gain more insight, AMP-CPP (or buffer as control) was preincubated with RdRp·RNA binary complexes for 5 min to trap the "closed" state by forming RdRp·RNA·AMP-CPP ternary complexes, and then the reaction was initiated by the addition of an excess amount of ATP (Fig. 9). The reaction occurs only when AMP-CPP is exchanged with ATP. The rate for nucleotide incorporation was determined with and without AMP-CPP. The delay in nucleotide incorporation induced by AMP-CPP is a measure of the reverse rate of the prechemistry conformational change. For WT and K167R RdRps, the rates were delayed by 40–50-fold (Fig. 9). However, in R174K RdRp, the rate was delayed by only 3-fold (Fig. 9). These results suggested that the R174K substitution destabilized the "closed" state of the ternary complex, consistent with the NMR experiments (Figs. 4–6). The slower rate of catalysis together with the enhanced ability to exchange nucleotides probably provide additional opportunities for the R174K variant to release incorrect nucleotide, leading to a higher fidelity enzyme.

The Functional Roles of Arg-174 and Lys-359 Are Largely Independent—It was shown previously that the K359R and K359L substitutions lead to decreases in k_{pol} and increases in polymerase fidelity (5, 12, 13). Because both Arg-174 and Lys-359 (13) appear to be important for the conformational changes in motif D observed by NMR (Fig. 5), we wanted to understand whether the roles of these residues were related or independent from one another. To address this question, we compared the kinetics of the variants with single amino acid substitutions (*i.e.* R174K and K359L) with the variant with both amino acid substitutions (*i.e.* R174K/K359L). RdRp with a nonpolar residue at position 359 (*i.e.* K359M) does not undergo the same conformational changes as WT enzyme (13), similar to what is observed for the R174K variant (Fig. 5). The R174K/K359L variant demonstrated decreased affinity to RNA (Table 2) and was much more impaired in its ability to incorporate correct ATP

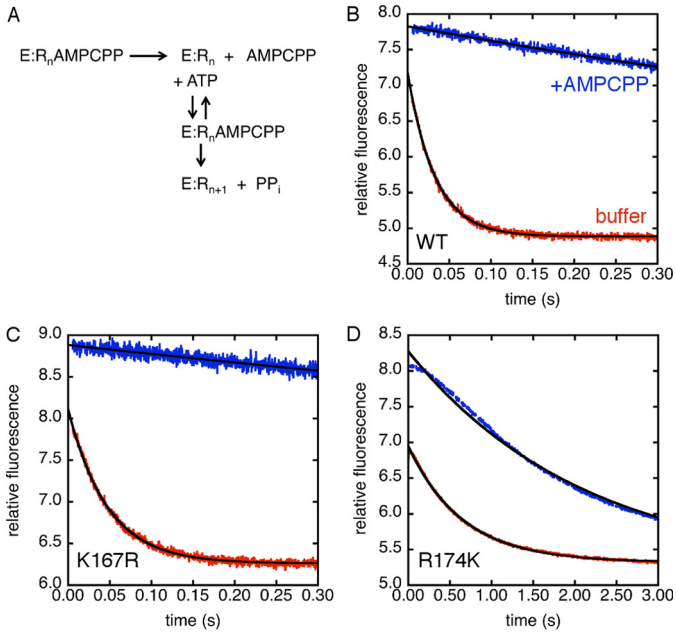

FIGURE 9. **The R174K substitution destabilizes the "closed" conformation.** *A*, the minimal kinetic mechanism for the dissociation of AMP-CPP and incorporation of AMP. Reactions contained 50 mM HEPES, pH 7.5, 10 mM β-mercaptoethanol, 5 mM $MnCl_2$, and 60 μM $ZnCl_2$. Enzyme was preincubated with sym/sub-UA to form binary complexes for 90 s. Then 200 μM AMP-CPP or buffer was added and incubated for an extra 5 min to form RdRp·RNA·AMP-CPP ternary complexes. Reactions were initiated by the addition of an excess amount of ATP. AMP incorporation was then monitored by fluorescent changes using a stopped flow apparatus. Final concentrations of ATP, sym/sub-UA, and RdRp were 1 mM, 1 μM (WT and K167R) or 2 μM (R174K), and 1 μM, respectively. *B–D*, the comparison of AMP incorporation in the presence (*blue*) and absence (*red*) of AMP-CPP for WT (*B*), K167R (*C*), and R174K RdRp (*D*). The *black solid lines* represent fits of the data to single exponential curves.

nucleotide compared with either of the two single variants (Table 1).

To test whether the amino acid substitutions were thermodynamically coupled and hence whether the function of the residues were interdependent, we compared the free energy changes induced in the catalytic efficiency (*i.e.* $\Delta\Delta G = -RT \ln ((k_{pol}/K_{d(app)})_{variant}/(k_{pol}/K_{d(app)},app)_{WT})$ by the single and double amino acid substitutions, analogous to the classic double mutant cycle experiments performed by Fersht (38), Mildvan *et al.* (39), and Serrano *et al.* (40). The effects of the R174K ($\Delta\Delta G$ = 1.2 kcal/mol) and K359L ($\Delta\Delta G$ = 4.0 kcal/mol) substitutions were nearly additive (assuming ~20% error) compared with the R174K/K359L double amino acid substitution ($\Delta\Delta G$ = 6.0 kcal/mol), suggesting that these residues are very weakly thermodynamically coupled and that their roles are largely independent from one another. If the functions of these residues were interrelated, we would have expected a non-additive response. The differences in the NMR spectra for the R174K and K359R variants also suggest that these amino acid substitutions have substantially different effects on the nucleotide and protein structural dynamics.

Fidelity Variants Substantially Alter Triphosphate Binding and Reorientation—Our NMR and kinetic studies indicated that amino acid substitutions at residues that interact with the NTP triphosphate lead to changes in catalytic efficiency and polymerase fidelity. We were interested in testing whether other amino acid substitutions that change polymerase fidelity

and attenuate the virus also lead to changes to the triphosphate-binding environment. In particular, the G64S and H273R substitutions are relatively remote from the active site (×20 Å away from the catalytic center) but generate higher and lower fidelity polymerases, respectively (41–43). Although these amino acid changes are relatively remote from the active site, interaction pathways suggest how these substitutions might affect RdRp catalysis and fidelity. For example, Gly-64 is involved in a hydrogen bonding network involving Ala-239 and Leu-241 in motif A and Gly-285 in motif B. His-273 makes hydrogen bond interactions with Thr-156 in a β-strand that makes interactions with the β-strand containing Arg-174. MD simulations have also shown how the G64S and H273R substitutions affect structural dynamics around the active site and more globally (22, 44). Another intriguing fidelity variant is T362I RdRp (18). We were initially interested in this amino acid substitution because it is encoded by the Sabin I vaccine strain and is located in motif D, near Lys-359 (45). Our studies indicated that the T362I substitution leads to a lower fidelity polymerase, probably because it can access a more active conformation even in the presence of incorrect nucleotide (18). The T362I substitution by itself (*i.e.* in the absence of other Sabin I mutations) also leads to some attenuation of the encoding PV strain (18). In the presence of other Sabin I substitutions, these effects are largely mitigated (46). Nonetheless, the T362I variant can serve as an important tool in understanding how the conformational dynamics of motif D are (un)related to the realignment of the triphosphate.

We assessed protein structural changes in the G64S, H273R, and T362I variants by using [*methyl*-^{13}C]Met NMR. We were especially interested in tracking the Met-354 resonance, as it responds to structural changes in motif D and surrounding areas (Fig. 1). The G64S substitution induced only very small chemical shift differences in the [*methyl*-^{13}C]Met spectra for the RdRp·RNA·UTP, RdRp·RNA·2′-dUTP, and RdRp·RNA·CTP complexes (Fig. 10*A*) compared with WT RdRp (Fig. 5). In contrast, the H273R·RNA·2′-dUTP, T362I·RNA·2′-dUTP, and T362I·RNA·CTP complexes all led to spectral changes compared with the same WT and G64S complexes (Fig. 10, *B* and *C*). We had previously noted that the T362I variant gives rise to two sets of resonances for the RdRp·RNA·2′-dUTP complex (18); one set of resonances overlaps what is observed for the WT·RNA·UTP complex, and the other set of resonances overlaps what is observed for the WT·RNA·CTP complex. This finding prompted us to suggest that the T362I variant can access a more active conformation even in the presence of the incorrect 2′-dUTP (18), suggesting why it is a lower fidelity variant. The T362I·RNA·CTP complex also appeared to fluctuate into two (or more) conformations, considering the presence of two Met-354 resonances.

Our previous studies also highlighted the effects of these substitutions on the Met-187 resonance, as a reporter on motif B and surrounding regions (22). The G64S spectra were similar to those of WT RdRp (22). As mentioned previously, the Met-187 resonances for the RdRp·RNA, RdRp·RNA·UTP, and RdRp·RNA·CTP complexes for the H273R variant all overlapped, consistent with the H273R substitution stabilizing the NTP binding-competent conformation, helping to bypass this fidelity checkpoint (22). For T362I, the Met-187 resonance for

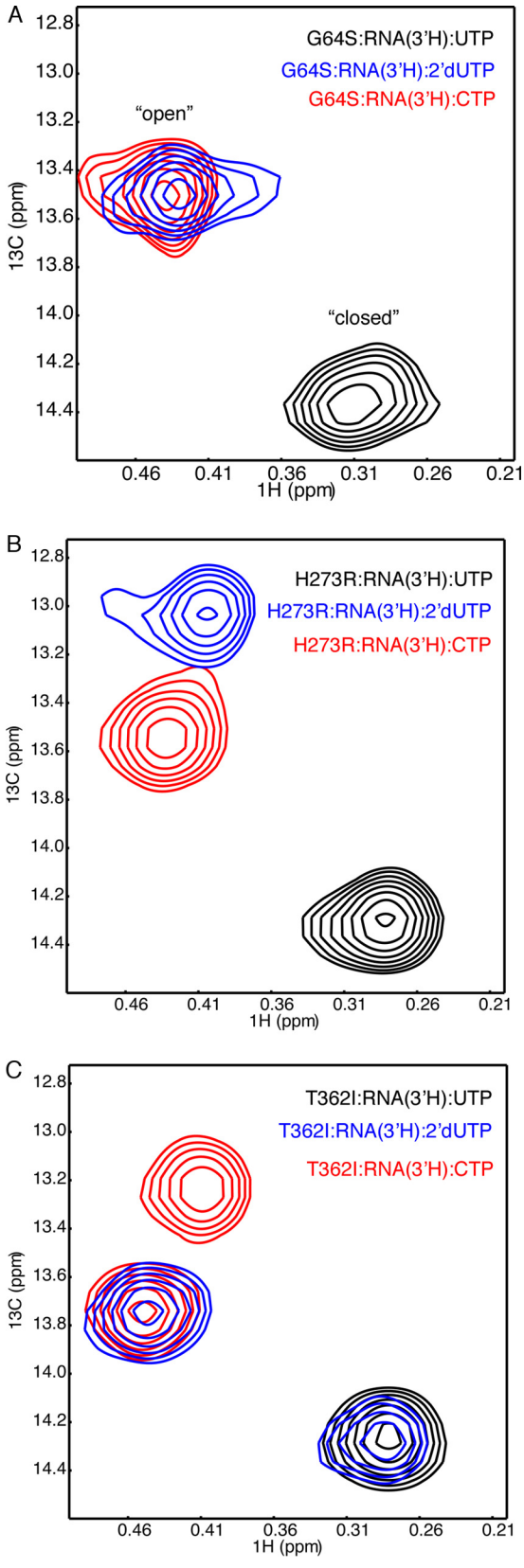

FIGURE 10. **Fidelity variants of RdRp can change the conformational dynamics of motif D.** *A–C*, *close-ups* of [*methyl*-^{13}C]Met HSQC spectra showing the Met-354 resonances for WT, H273R, and T362I RdRp bound with RNA lacking a 3′-OH and correct UTP nucleotide (*black*) or incorrect 2′-dUTP (*blue*) or incorrect CTP (*red*) nucleotide. Spectra were collected at 293 K using 250 μM RdRp with 500 μM RNA and 4 mM UTP, 8 mM 2′-dUTP, or 12 mM CTP and a D_2O-based buffer consisting of 10 mM HEPES, pH 8.0, 200 mM NaCl, 0.02% NaN_3, 5 mM MgCl, and 10 μM ZnCl.

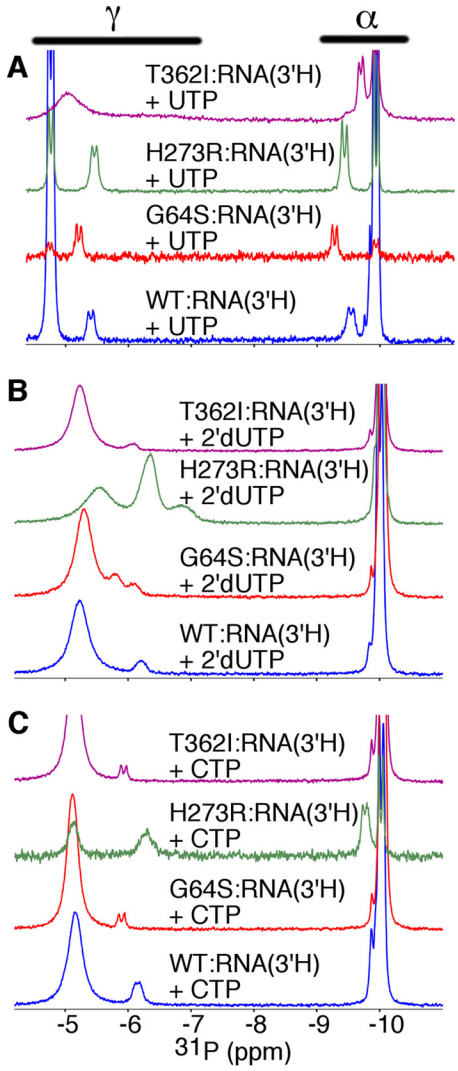

FIGURE 11. **Lower and higher fidelity RdRp variants change the orientation and/or microenvironment of the triphosphate for the incoming nucleotide.** Comparisons of RdRp·RNA complexes bound with correct nucleotide (*i.e.* UTP) (*A*), bound with incorrect nucleotide with incorrect sugar (*i.e.* 2′-dUTP) (*B*), and bound with incorrect nucleotide with incorrect nucleobase (*i.e.* CTP) (*C*) for WT (*black*), G64S (*red*), H273R (*green*), and T362I (*blue*) RdRp. The G64S substitution leads to a higher fidelity polymerase (41), and the H273R (22) and T362I (18) substitutions lead to lower fidelity polymerases. Spectra were collected at 303 K with 250 μM RdRp, 500 μM RNA, 3.1 mM 3′-dATP, and 4 mM UTP, 8 mM 2′-dUTP, or 12 mM CTP and a buffer consisting of 10 mM HEPES, pH 8.0, 200 mM NaCl, 0.02% NaN_3, 5 mM MgCl, and 10 μM ZnCl.

the RdRp·RNA·UTP complex was similar to that for WT enzyme, but the Met-187 resonance for the RdRp·RNA·CTP complex was at a chemical shift position different from that for WT RdRp (22).

To test the effects of the G64S, H273R, and T362I substitutions on the binding and microenvironment of the NTP triphosphate, we collected ^{31}P NMR spectra of their correct RdRp·RNA·UTP and incorrect RdRp·RNA·2′-dUTP and RdRp·RNA·CTP complexes (Fig. 11). It should be kept in mind that any changes in the ^{31}P NMR spectra of the G64S, H273R, and T362I variants must be due to indirect effects, because these residues do not make direct interactions with RNA or NTP. Nonetheless, there were substantial changes in the ^{31}P NMR spectra for these variants compared with WT RdRp, especially for the G64S and H273R variants (Fig. 11). In particular, the H273R substitution induced chemical shift changes for the α-P and γ-P peaks in the RdRp·RNA·UTP complex (Fig. 11*A*), suggesting that correct nucleotide may bind in a different manner, and/or the surrounding microenvironment has been altered in the H273R variant. These effects might be due to the series of interactions connecting His-273 to the β-strand containing Arg-174, as suggested above, and/or changes in the structural dynamics around the active site, as observed previously in MD simulations (22).

There were also differences in the ^{31}P spectra for the G64S and H273R variants in their respective RdRp·RNA·2′-dUTP and RdRp·RNA·CTP complexes compared with WT enzyme (Fig. 11, *B* and *C*). Intriguingly, both G64S and H273R variants gave rise to additional γ-P peaks in the RdRp·RNA·2′-dUTP complexes. We do not think these additional peaks correspond to additional binding pockets created by these variants because these substitutions are not on the surface or near any binding sites. Instead, we suggest that these additional peaks probably correspond to the γ-phosphate of protein-bound 2′-dUTP fluctuating between different conformations and/or microenvironments. In the G64S·RNA·CTP complex, the γ-P peak for the G64S variant was downfield shifted (δ −5.87 ppm) and appeared to be more well resolved (*i.e.* the doublet was apparent) compared with what is observed for WT RdRp (Fig. 11*C*). These findings suggest that the binding environment and/or conformational dynamics of the triphosphate in the G64S variant are different from those of WT RdRp. Likewise, the H273R substitution also led to chemical shift differences in the α-P (δ −9.77 ppm) and γ-P (δ −6.30 ppm) peaks for the RdRp·RNA·CTP complex, although these changes were distinct from what was observed in the G64S variant (Fig. 11*C*). Most notably, there was less of a difference in the chemical shift of the α-P peaks between the RdRp·RNA·CTP and RdRp·RNA·UTP complexes (δ −9.46 ppm) compared with the same complexes for WT enzyme. This result might suggest that the α-phosphates for these complexes were in more comparable chemical environments for the H273R variant compared with WT RdRp. If true, this finding would help to explain why the H273R variant has a lower ability to discriminate between correct and incorrect nucleotides. This result is also consistent with the proposal that the H273R substitution stabilizes the NTP-binding competent conformation, helping to bypass this fidelity checkpoint (22).

In contrast to what is observed for the G64S and H273R variants, the T362I substitution did not lead to additional γ-P peaks for the RdRp·RNA·2′-dUTP complex. In fact, the ^{31}P spectrum was very similar to that for WT RdRp (Fig. 11), which was in stark contrast to the corresponding [*methyl*-^{13}C]Met spectra (Fig. 8). The T362I substitution also induced a chemical shift change in the γ-P peak (δ −5.90 ppm) compared with what was observed for the WT enzyme (Fig. 11*C*), although this might just reflect a change in the CTP exchange kinetics on/off the enzyme (*i.e.* the γ-P peaks are less broad and more intense for the T362I variant). The T362I substitution also induced changes in the RdRp·RNA·UTP spectra, which was a bit surprising considering that the corresponding [*methyl*-^{13}C]Met spectra were very similar to WT enzyme. These findings sug-

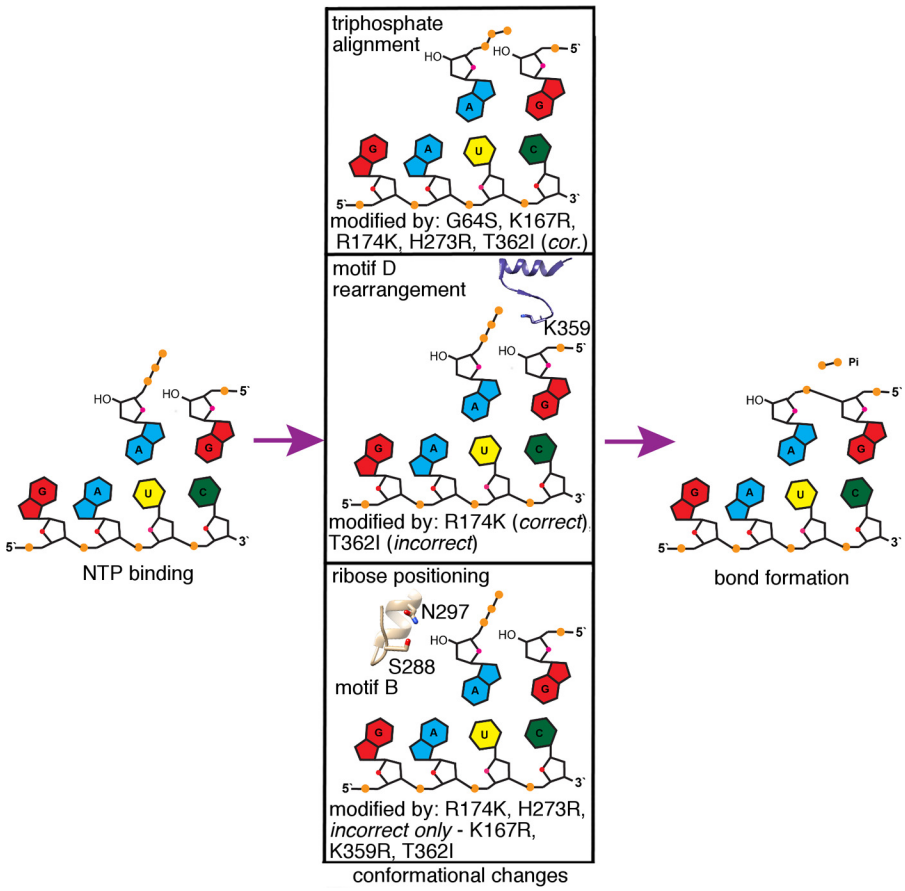

FIGURE 12. **Nucleotide selection checkpoints altered by PV RdRp fidelity variants.** Conformational changes important for nucleotide incorporation include a reorientation of the triphosphate of the incoming nucleotide for direct in-line attack by the RNA 3′-OH, a conformational change in structural motif D to reposition conserved residue Lys-359, and conformational changes in structural motif B to allow for interactions with the 2′-OH of the incoming nucleotide. We have developed diagnostic NMR probes for each of these rearrangements; our ^{31}P NMR studies provide insight into the environment surrounding the triphosphate of the incoming nucleotide, and our [*methyl*-^{13}C]Met NMR studies provide probes for structural changes in motifs B (*i.e.* Met-187) and D (*i.e.* Met-354). Our results indicate that the fidelity-altering amino acid substitutions differentially affect these checkpoints, suggesting that the checkpoints are not strictly dependent on each other.

gest that the T362I substitution can have differing effects on the NTP triphosphate and motif B/D structural dynamics.

Discussion

Enzymes within the nucleic acid polymerase superfamily appear to share a common kinetic mechanism, including a conformational change into a more active form before catalyzing phosphodiester bond formation (1). There has been much debate over the structural details of this conformational change (47). It is likely that the prechemistry conformational change identified in these kinetic mechanisms actually represents a number of conformational events. In RdRps, there are structural rearrangements in motifs A and B to interact with the NTP ribose hydroxyls, a realignment of the NTP triphosphate for proper orientation, and a repositioning of the motif D lysine (Lys-359 in PV RdRp) to act as a general acid to protonate the pyrophosphate leaving group. We have now developed diagnostic NMR experiments to probe each of these structural changes, allowing us to investigate the nucleotide incorporation cycle for WT and fidelity-altering variants. Specifically, the ^{31}P NMR experiments that we have developed here probe the binding environment of the NTP triphosphate, and our previously developed [*methyl*-^{13}C]Met probes monitor structural changes in motifs B and D (Fig. 1*C*) and surrounding areas. Our studies provide insight into not only which fidelity checkpoints are altered by these amino acid substitutions, but provide information about the connections between different fidelity checkpoints through comparisons of fidelity variants (Fig. 12).

In this report, we have developed a ^{31}P NMR assay to probe the binding environment of the NTP triphosphate (Fig. 2). Crystal structures of nucleic acid polymerase superfamily members have indicated that there is a reorientation of the triphosphate of the incoming nucleotide following initial binding to properly align the α-phosphate for nucleophilic attack by the primer 3′-OH (10, 48) (Fig. 12). Having a mispaired primer terminus and/or binding incorrect nucleotide does not result in the same structural rearrangement (32–34, 49). As such, the reorientation of the triphosphate probably reflects an important fidelity checkpoint (10, 37, 50–52). Our ^{31}P NMR studies on PV RdRp are consistent with these proposals, where the binding of correct and incorrect NTP led to different ^{31}P NMR signatures (Figs. 3 and 4). In the interpretation of these experiments, it should be kept in mind that the spectra can represent a mixture of states. If the triphosphate is fluctuating between different conformations on a time scale fast relative to the chemical shift differences between these states, we would

observe only a single set of peaks for protein-bound NTP that represents a weighted average of these different states. Changing residues proposed to interact with the NTP triphosphate led to changes in rates and fidelity of nucleotide addition (Table 1). Interestingly, modification of Arg-174 and Lys-359, proposed to interact with the α- and β-phosphates, respectively, increased fidelity, whereas modification of Lys-167, proposed to interact with the γ-phosphate, decreased fidelity. The SDKIE and metal effects suggested that these modifications primarily affected the chemistry step itself.

We have also suggested that conformational changes to reposition Lys-359 for catalysis, analogous to the conformational change in the O/P helix in the A/B family DNA polymerases (32, 34, 53–61), represent an important fidelity checkpoint. The Met-354 resonance has been diagnostic of conformational changes in motif D (13, 21) (Figs. 1*C* and 5). The chemical shift changes experienced by Met-354 are absolutely dependent on the protonation state of Lys-359 (13); only under conditions in which the side-chain amine of Lys-359 is protonated do these structural changes occur. We do not observe similar chemical shift changes upon binding incorrect nucleotide. Consistent with this proposal, the K359R substitution changed the ^{31}P NMR spectrum relative to WT for the correct RdRp·RNA·UTP complex but not for the incorrect RdRp·RNA·CTP complex (Fig. 4). This result suggested that this residue was only brought near the NTP triphosphate when correct NTP was present. Unfortunately, PV RdRp crystal structures have failed to capture Lys-359 in a position to protonate the pyrophosphate leaving group. We note here that the ^{31}P and ^{1}H-^{13}C spectra (Figs. 4 and 5) and the AMP-CPP trap assay (Fig. 9) indicated that the R174K variant was impaired in its ability to fluctuate into a closed conformation. These results might indicate that R174K is capable of catalyzing phosphodiester bond formation through an open-like conformation (*i.e.* when Lys-359 is not in a position to donate a proton to the β-phosphate). Likewise, catalysis in the RdRp crystals may not require the repositioning of Lys-359. It is known that Lys-359 is not absolutely required for catalysis, considering that amino acid substitutions at this position only decrease the catalytic rate by up to 50-fold (12).

Structural rearrangements in motifs A/B upon interacting with the NTP ribose are also well known to be important for RdRp fidelity (62). The Met-187 resonance serves as a diagnostic probe for structure/dynamic changes in motif B and surrounding areas (Fig. 1*C*). It is intriguing that most of the fidelity variants resulted in some change to the Met-187 resonances (Fig. 6) (22). The pervasiveness of these changes to Met-187 and its surrounding environment are consistent with motif A/B-ribose interactions being one of the first steps in NTP binding and selection, necessary to trigger subsequent conformational changes.

One question regarding RdRp fidelity is whether these fidelity checkpoints, involving structural changes in motifs A/B induced by interacting with the NTP ribose, rearrangement of the NTP triphosphate, and repositioning of the general acid Lys-359, are interdependent. Our NMR and kinetic analyses suggest that fidelity-altering substitutions have differing, potentially independent effects on these checkpoints. For example, fidelity variants may change interactions with the NTP triphosphate or lead to structure/dynamic changes in motif D, but not necessarily both (Fig. 12). In these cases, it appears that changes in the NTP triphosphate binding/conformation and structure/dynamics in motif D are not strictly coupled. For instance, there were additional γ-P peaks for the G64S·RNA·2′-dUTP and H273R·RNA·2′-dUTP complexes (Fig. 11), but these were not accompanied by additional peaks in the [*methyl*-^{13}C]Met spectra (Fig. 10). Likewise, there were additional resonances in the [*methyl*-^{13}C]Met spectra, but not the ^{31}P spectra, for the T362I·RNA·2′-dUTP and T362I·RNA·CTP complexes. These results were also consistent with the finding that amino acid substitutions at Arg-174 and Lys-359 were not thermodynamically coupled, according to double mutant cycle analysis (Table 1). Likewise, the behavior (*i.e.* chemical shift, number of resonances) of the Met-187 resonance(s) (Fig. 6) (22) was not coupled to what was observed for the Met-354 resonance (Figs. 5 and 10) or the ^{31}P triphosphate spectra (Figs. 4 and 11).

Altogether, our results are consistent with the proposal that the realignment of the NTP triphosphate is an important fidelity checkpoint, but this event is not strictly coupled to other fidelity checkpoints in the RdRp (Fig. 12). This finding is especially interesting in comparison with what is found in the A/B family DNA polymerases, in which the positively charged residues that interact with the NTP triphosphate are all located on or near the O/P helix. In RdRps, it appears that the positively charged amino acids interacting primarily with the α- and γ-phosphates (*e.g.* Lys-167 and Arg-174 in motif F) are segregated from the positively charged residue that interacts with the β-phosphate and acts as the general acid (*i.e.* Lys-359 on motif D). Our findings suggest that the binding and alignment of the triphosphate necessary for the bond formation between the α-phosphate and the primer 3′-O group are effectively separated in time and space from the repositioning of the general acid whose actions facilitate bond breakage between the α- and β-phosphates. The separation of these fidelity checkpoints probably allows independent verification of the incoming NTP, which might be especially important for polymerases that lack proofreading domains.

Experimental Procedures

Materials—[γ-^{32}P]ATP (>7000 Ci/mmol) was from VWR-MP Biomedical; nucleoside 5′-triphosphates and 2′-deoxynucleoside 5′-triphosphates (all nucleotides were ultrapure solutions) were from GE Healthcare; 3′-deoxyadenosine 5′-triphosphate was from Trilink Biotechnologies. All RNA oligonucleotides were from Dharmacon Research, Inc. (Boulder, CO). [*methyl*-^{13}C]Methionine was from Cambridge Isotope Laboratories. All other reagents were of the highest grade available from Sigma or Fisher.

Site-directed Mutagenesis, Protein Overexpression, and Purification of PV RdRp—All mutants were generated using the QuikChange method (Stratagene) and appropriate primers. Mutations were confirmed by DNA sequencing (Nucleic Acid Facility, Pennsylvania State University). It should be noted that WT and all variant RdRps also have L446D and R455D substitutions to prevent RdRp self-association. Overexpression and

purification of PV RdRp followed procedures described previously (21, 23, 63, 64).

NMR Sample Preparation and Spectroscopy—NMR samples of the different complexes (free protein, bound to RNA, bound to RNA and NTP, and so on) were prepared as described previously (13, 21). The NMR buffer consists of 10 mM HEPES, pH 8.0, 200 mM NaCl, 0.02% NaN_3, 5 mM MgCl, and 10 μM ZnCl. For ϵ-$^{13}CH_3$ Met-labeled protein, samples were in 100% D_2O, but samples generated for ^{31}P NMR contained 90% H_2O and 10% D_2O for the lock signal. Data collection for the ϵ-$^{13}CH_3$ Met-labeled samples followed previous procedures (13, 21).

The ^{31}P NMR spectra were collected using a Bruker Avance III 600-MHz NMR spectrometer with a ^{31}P-selective probe at spectrometer frequencies of 600.07 MHz for ^{1}H and 242.91 MHz for ^{31}P. The experiments were performed with fully calibrated 90° pulses and used a recycle delay of 1 s to suppress signal from free-floating RNA and NTP. Protons were decoupled during data acquisition using the Waltz16 sequence. The ^{31}P chemical shifts are expressed with reference to an 85% phosphoric acid external standard.

RNA Binding Assays—Fluorescence polarization assays were conducted to determine sym/sub-UA binding affinity of variant and WT RdRp. Reactions contained 50 mM HEPES, pH 7.5, 10 mM 2-mercaptoethanol, 5 mM $MgCl_2$, 60 μM $ZnCl_2$, and 10 mM NaCl. Reactions were conducted at room temperature. Enzyme was added immediately from ice, and minipolarization was measured after 10 min from the addition to reach the binding equilibrium. The sym/sub-UA was modified with 6-FAM at the 5′-end of the oligonucleotide. The concentration of 6-FAM-sym/sub-UA was 1 nM. The volume of enzyme added into the reaction was no more than one-tenth of the total assay volume.

Enzyme Kinetic Assays—Enzyme assays, including active-site titration assays, RdRp·RNA·NTP assembly assays, and RdRp·RNA dissociation assays, were conducted as described previously (18, 23). The reactions contained 50 mM HEPES, pH 7.5, 10 mM 2-mercaptoethanol, 5 mM $MgCl_2$, and 60 μM $ZnCl_2$. The stopped flow experiments and the benchtop assays for nucleotide incorporations were conducted as described previously (18). Reactions were incubated at 30 °C and were quenched by the addition of an equal volume of EDTA to a final concentration of 25 mM. Specific concentrations of RdRp, sym/sub-UA, and nucleotide are indicated in the corresponding figure legends.

Author Contributions—X. Y., X. L., J. J. A., C. E. C., and D. D. B. designed the study and wrote the paper. X. Y. collected and analyzed the NMR data. X. L. performed and analyzed the kinetic studies. D. M. M. helped in the purification and NMR characterization of the proteins. I. M. M. helped to design Figs. 1 and 12. All authors analyzed the results and approved the final version of the manuscript.

References

1. Trakselis, M. A., and Murakami, K. S. (2014) Introduction to nucleic acid polymerases: families, themes and mechanisms. *Nucleic Acids Mol. Biol.* **30,** 1–15
2. Pfeiffer, J. K., and Kirkegaard, K. (2005) Increased fidelity reduces poliovirus fitness and virulence under selective pressure in mice. *PLoS Pathog.* **1,** e11
3. Vignuzzi, M., Stone, J. K., Arnold, J. J., Cameron, C. E., and Andino, R. (2006) Quasispecies diversity determines pathogenesis through cooperative interactions in a viral population. *Nature* **439,** 344–348
4. Vignuzzi, M., Wendt, E., and Andino, R. (2008) Engineering attenuated virus vaccines by controlling replication fidelity. *Nat. Med.* **14,** 154–161
5. Weeks, S. A., Lee, C. A., Zhao, Y., Smidansky, E. D., August, A., Arnold, J. J., and Cameron, C. E. (2012) A polymerase mechanism-based strategy for viral attenuation and vaccine development. *J. Biol. Chem.* **287,** 31618–31622
6. Gnädig, N. F., Beaucourt, S., Campagnola, G., Bordería, A. V., Sanz-Ramos, M., Gong, P., Blanc, H., Peersen, O. B., and Vignuzzi, M. (2012) coxsackievirus B3 mutator strains are attenuated *in vivo*. *Proc. Natl. Acad. Sci. U.S.A.* **109,** E2294–E2303
7. Graci, J. D., and Cameron, C. E. (2008) Therapeutically targeting RNA viruses via lethal mutagenesis. *Future Virol.* **3,** 553–566
8. Gong, P., Kortus, M. G., Nix, J. C., Davis, R. E., and Peersen, O. B. (2013) Structures of coxsackievirus, rhinovirus, and poliovirus polymerase elongation complexes solved by engineering RNA mediated crystal contacts. *PLoS One* **8,** e60272
9. Gong, P., and Peersen, O. B. (2010) Structural basis for active site closure by the poliovirus RNA-dependent RNA polymerase. *Proc. Natl. Acad. Sci. U.S.A.* **107,** 22505–22510
10. Shu, B., and Gong, P. (2016) Structural basis of viral RNA-dependent RNA polymerase catalysis and translocation. *Proc. Natl. Acad. Sci. U.S.A.* **113,** E4005–E4014
11. Castro, C., Smidansky, E., Maksimchuk, K. R., Arnold, J. J., Korneeva, V. S., Götte, M., Konigsberg, W., and Cameron, C. E. (2007) Two proton transfers in the transition state for nucleotidyl transfer catalyzed by RNA- and DNA-dependent RNA and DNA polymerases. *Proc. Natl. Acad. Sci. U.S.A.* **104,** 4267–4272
12. Castro, C., Smidansky, E. D., Arnold, J. J., Maksimchuk, K. R., Moustafa, I., Uchida, A., Götte, M., Konigsberg, W., and Cameron, C. E. (2009) Nucleic acid polymerases use a general acid for nucleotidyl transfer. *Nat. Struct. Mol. Biol.* **16,** 212–218
13. Yang, X., Smidansky, E. D., Maksimchuk, K. R., Lum, D., Welch, J. L., Arnold, J. J., Cameron, C. E., and Boehr, D. D. (2012) Motif D of viral RNA-dependent RNA polymerases determines efficiency and fidelity of nucleotide addition. *Structure* **20,** 1519–1527
14. Castro, C., Arnold, J. J., and Cameron, C. E. (2005) Incorporation fidelity of the viral RNA-dependent RNA polymerase: a kinetic, thermodynamic and structural perspective. *Virus Res.* **107,** 141–149
15. Gohara, D. W., Arnold, J. J., and Cameron, C. E. (2004) Poliovirus RNA-dependent RNA polymerase (3Dpol): kinetic, thermodynamic, and structural analysis of ribonucleotide selection. *Biochemistry* **43,** 5149–5158
16. Gohara, D. W., Crotty, S., Arnold, J. J., Yoder, J. D., Andino, R., and Cameron, C. E. (2000) Poliovirus RNA-dependent RNA polymerase (3Dpol): structural, biochemical, and biological analysis of conserved structural motifs A and B. *J. Biol. Chem.* **275,** 25523–25532
17. Korneeva, V. S., and Cameron, C. E. (2007) Structure-function relationships of the viral RNA-dependent RNA polymerase: fidelity, replication speed, and initiation mechanism determined by a residue in the ribose-binding pocket. *J. Biol. Chem.* **282,** 16135–16145
18. Liu, X., Yang, X., Lee, C. A., Moustafa, I. M., Smidansky, E. D., Lum, D., Arnold, J. J., Cameron, C. E., and Boehr, D. D. (2013) Vaccine-derived mutation in motif D of poliovirus RNA-dependent RNA polymerase lowers nucleotide incorporation fidelity. *J. Biol. Chem.* **288,** 32753–32765
19. McDonald, S., Block, A., Beaucourt, S., Moratorio, G., Vignuzzi, M., and Peersen, O. B. (2016) Design of a genetically stable high fidelity coxsackievirus B3 polymerase that attenuates virus growth *in vivo*. *J. Biol. Chem.* **291,** 13999–14011
20. Curti, E., and Jaeger, J. (2013) Residues Arg283, Arg285, and Ile287 in the nucleotide binding pocket of bovine viral diarrhea virus NS5B RNA polymerase affect catalysis and fidelity. *J. Virol.* **87,** 199–207
21. Yang, X., Welch, J. L., Arnold, J. J., and Boehr, D. D. (2010) Long-range interaction networks in the function and fidelity of poliovirus RNA-de-

pendent RNA polymerase studied by nuclear magnetic resonance. *Biochemistry* **49,** 9361–9371
22. Moustafa, I. M., Korboukh, V. K., Arnold, J. J., Smidansky, E. D., Marcotte, L. L., Gohara, D. W., Yang, X., Sánchez-Farrán, M. A., Filman, D., Maranas, J. K., Boehr, D. D., Hogle, J. M., Colina, C. M., and Cameron, C. E. (2014) Structural dynamics as a contributor to error-prone replication by an RNA-dependent RNA polymerase. *J. Biol. Chem.* **289,** 36229–36248
23. Arnold, J. J., and Cameron, C. E. (2000) Poliovirus RNA-dependent RNA polymerase (3D(pol)): assembly of stable, elongation-competent complexes by using a symmetrical primer-template substrate (sym/sub). *J. Biol. Chem.* **275,** 5329–5336
24. Cohn, M., and Hughes, T. R., Jr. (1962) Nuclear magnetic resonance spectra of adenosine di- and triphosphate. II. Effect of complexing with divalent metal ions. *J. Biol. Chem.* **237,** 176–181
25. Sloan, D. L., Loeb, L. A., and Mildvan, A. S. (1975) Conformation of deoxynucleoside triphosphate substrates on DNA polymerase I from *Escherichia coli* as determined by nuclear magnetic relaxation. *J. Biol. Chem.* **250,** 8913–8920
26. Gupta, R. K., and Mildvan, A. S. (1977) Structures of enzyme-bound metal-nucleotide complexes in the phosphoryl transfer reaction of muscle pyruvate kinase: ^{31}P NMR studies with magnesium and kinetic studies with chromium nucleotides. *J. Biol. Chem.* **252,** 5967–5976
27. Rao, B. D., Cohn, M., and Scopes, R. K. (1978) ^{31}P NMR study of bound reactants and products of yeast 3-phosphoglycerate kinase at equilibrium and the effect of sulfate ion. *J. Biol. Chem.* **253,** 8056–8060
28. Bock, J. L. (1980) The binding of metal ions to ATP: a proton and phosphorus nmr investigation of diamagnetic metal-ATP complexes. *J. Inorg. Biochem.* **12,** 119–130
29. Furukawa, A., Konuma, T., Yanaka, S., and Sugase, K. (2016) Quantitative analysis of protein-ligand interactions by NMR. *Prog. Nucl. Magn. Reson. Spectrosc.* **96,** 47–57
30. Kirmizialtin, S., Nguyen, V., Johnson, K. A., and Elber, R. (2012) How conformational dynamics of DNA polymerase select correct substrates: experiments and simulations. *Structure* **20,** 618–627
31. Beard, W. A., and Wilson, S. H. (2003) Structural insights into the origins of DNA polymerase fidelity. *Structure* **11,** 489–496
32. Wu, E. Y., and Beese, L. S. (2011) The structure of a high fidelity DNA polymerase bound to a mismatched nucleotide reveals an "ajar" intermediate conformation in the nucleotide selection mechanism. *J. Biol. Chem.* **286,** 19758–19767
33. Wang, W., Wu, E. Y., Hellinga, H. W., and Beese, L. S. (2012) Structural factors that determine selectivity of a high fidelity DNA polymerase for deoxy-, dideoxy-, and ribonucleotides. *J. Biol. Chem.* **287,** 28215–28226
34. Johnson, S. J., and Beese, L. S. (2004) Structures of mismatch replication errors observed in a DNA polymerase. *Cell* **116,** 803–816
35. Freudenthal, B. D., Beard, W. A., Shock, D. D., and Wilson, S. H. (2013) Observing a DNA polymerase choose right from wrong. *Cell* **154,** 157–168
36. Arnold, J. J., and Cameron, C. E. (2004) Poliovirus RNA-dependent RNA polymerase (3Dpol): pre-steady-state kinetic analysis of ribonucleotide incorporation in the presence of Mg^{2+}. *Biochemistry* **43,** 5126–5137
37. Arnold, J. J., Gohara, D. W., and Cameron, C. E. (2004) Poliovirus RNA-dependent RNA polymerase (3Dpol): pre-steady-state kinetic analysis of ribonucleotide incorporation in the presence of Mn^{2+}. *Biochemistry* **43,** 5138–5148
38. Fersht, A. R. (1987) Dissection of the structure and activity of the tyrosyl-tRNA synthetase by site-directed mutagenesis. *Biochemistry* **26,** 8031–8037
39. Mildvan, A. S., Weber, D. J., and Kuliopulos, A. (1992) Quantitative interpretations of double mutations of enzymes. *Arch. Biochem. Biophys.* **294,** 327–340
40. Serrano, L., Horovitz, A., Avron, B., Bycroft, M., and Fersht, A. R. (1990) Estimating the contribution of engineered surface electrostatic interactions to protein stability by using double-mutant cycles. *Biochemistry* **29,** 9343–9352
41. Arnold, J. J., Vignuzzi, M., Stone, J. K., Andino, R., and Cameron, C. E. (2005) Remote site control of an active site fidelity checkpoint in a viral RNA-dependent RNA polymerase. *J. Biol. Chem.* **280,** 25706–25716
42. Korboukh, V. K., Lee, C. A., Acevedo, A., Vignuzzi, M., Xiao, Y., Arnold, J. J., Hemperly, S., Graci, J. D., August, A., Andino, R., and Cameron, C. E. (2014) RNA virus population diversity: an optimum for maximal fitness and virulence. *J. Biol. Chem.* **289,** 29531–29544
43. Moustafa, I. M., Shen, H., Morton, B., Colina, C. M., and Cameron, C. E. (2011) Molecular dynamics simulations of viral RNA-dependent RNA polymerases link conserved and correlated motions of functional elements to fidelity. *J. Mol. Biol.* **410,** 159–181
44. Marcotte, L. L., Wass, A. B., Gohara, D. W., Pathak, H. B., Arnold, J. J., Filman, D. J., Cameron, C. E., and Hogle, J. M. (2007) Crystal structure of poliovirus 3CD protein: virally encoded protease and precursor to the RNA-dependent RNA polymerase. *J. Virol.* **81,** 3583–3596
45. Nomoto, A., Omata, T., Toyoda, H., Kuge, S., Horie, H., Kataoka, Y., Genba, Y., Nakano, Y., and Imura, N. (1982) Complete nucleotide sequence of the attenuated poliovirus Sabin 1 strain genome. *Proc. Natl. Acad. Sci. U.S.A.* **79,** 5793–5797
46. Liu, X., Musser, D. M., Lee, C. A., Yang, X., Arnold, J. J., Cameron, C. E., and Boehr, D. D. (2015) Nucleobase but not sugar fidelity is maintained in the Sabin I RNA-dependent RNA polymerase. *Viruses* **7,** 5571–5586
47. Joyce, C. M., and Benkovic, S. J. (2004) DNA polymerase fidelity: kinetics, structure, and checkpoints. *Biochemistry* **43,** 14317–14324
48. Johnson, S. J., Taylor, J. S., and Beese, L. S. (2003) Processive DNA synthesis observed in a polymerase crystal suggests a mechanism for the prevention of frameshift mutations. *Proc. Natl. Acad. Sci. U.S.A.* **100,** 3895–3900
49. Wang, W., Hellinga, H. W., and Beese, L. S. (2011) Structural evidence for the rare tautomer hypothesis of spontaneous mutagenesis. *Proc. Natl. Acad. Sci. U.S.A.* **108,** 17644–17648
50. Kuchta, R. D., Mizrahi, V., Benkovic, P. A., Johnson, K. A., and Benkovic, S. J. (1987) Kinetic mechanism of DNA polymerase I (Klenow). *Biochemistry* **26,** 8410–8417
51. Ferrin, L. J., and Mildvan, A. S. (1985) Nuclear Overhauser effect studies of the conformations and binding site environments of deoxynucleoside triphosphate substrates bound to DNA polymerase I and its large fragment. *Biochemistry* **24,** 6904–6913
52. Ferrin, L. J., and Mildvan, A. S. (1986) NMR studies of conformations and interactions of substrates and ribonucleotide templates bound to the large fragment of DNA polymerase I. *Biochemistry* **25,** 5131–5145
53. Franklin, M. C., Wang, J., and Steitz, T. A. (2001) Structure of the replicating complex of a pol α family DNA polymerase. *Cell* **105,** 657–667
54. Kaushik, N., Pandey, V. N., and Modak, M. J. (1996) Significance of the O-helix residues of *Escherichia coli* DNA polymerase I in DNA synthesis: dynamics of the dNTP binding pocket. *Biochemistry* **35,** 7256–7266
55. Kiefer, J. R., Mao, C., Braman, J. C., and Beese, L. S. (1998) Visualizing DNA replication in a catalytically active *Bacillus* DNA polymerase crystal. *Nature* **391,** 304–307
56. Li, Y., Kong, Y., Korolev, S., and Waksman, G. (1998) Crystal structures of the Klenow fragment of *Thermus aquaticus* DNA polymerase I complexed with deoxyribonucleoside triphosphates. *Protein Sci.* **7,** 1116–1123
57. Li, Y., Korolev, S., and Waksman, G. (1998) Crystal structures of open and closed forms of binary and ternary complexes of the large fragment of *Thermus aquaticus* DNA polymerase I: structural basis for nucleotide incorporation. *EMBO J.* **17,** 7514–7525
58. Tahirov, T. H., Temiakov, D., Anikin, M., Patlan, V., McAllister, W. T., Vassylyev, D. G., and Yokoyama, S. (2002) Structure of a T7 RNA polymerase elongation complex at 2.9 Å resolution. *Nature* **420,** 43–50
59. Temiakov, D., Patlan, V., Anikin, M., McAllister, W. T., Yokoyama, S., and Vassylyev, D. G. (2004) Structural basis for substrate selection by t7 RNA polymerase. *Cell* **116,** 381–391
60. Yin, Y. W., and Steitz, T. A. (2002) Structural basis for the transition from initiation to elongation transcription in T7 RNA polymerase. *Science* **298,** 1387–1395

61. Yin, Y. W., and Steitz, T. A. (2004) The structural mechanism of translocation and helicase activity in T7 RNA polymerase. *Cell* **116,** 393–404
62. Garriga, D., Ferrer-Orta, C., Querol-Audí, J., Oliva, B., and Verdaguer, N. (2013) Role of motif B loop in allosteric regulation of RNA-dependent RNA polymerization activity. *J. Mol. Biol.* **425,** 2279–2287
63. Arnold, J. J., Bernal, A., Uche, U., Sterner, D. E., Butt, T. R., Cameron, C. E., and Mattern, M. R. (2006) Small ubiquitin-like modifying protein isopeptidase assay based on poliovirus RNA polymerase activity. *Anal. Biochem.* **350,** 214–221
64. Gohara, D. W., Ha, C. S., Kumar, S., Ghosh, B., Arnold, J. J., Wisniewski, T. J., and Cameron, C. E. (1999) Production of "authentic" poliovirus RNA-dependent RNA polymerase (3D(pol)) by ubiquitin-protease-mediated cleavage in *Escherichia coli*. *Protein Expr. Purif.* **17,** 128–138